Enhancing emulsification and encapsulation stability via Maillard reaction of garlic polysaccharide and casein for potent curcumin delivery emulsions

Xinyan Bai, Lingyu Li, X.G. Qiao, Wenqing Zhu, Yanna Hu, Laibing Sun, Marie-Laure Fauconnier, Zhenjia Zheng, Yiteng Qiao

PII: S0308-8146(25)02296-4

DOI: https://doi.org/10.1016/j.foodchem.2025.145045

Reference: FOCH 145045

To appear in: *Food Chemistry*

Received date: 17 January 2025

Revised date: 4 May 2025

Accepted date: 3 June 2025

Please cite this article as: X. Bai, L. Li, X.G. Qiao, et al., Enhancing emulsification and encapsulation stability via Maillard reaction of garlic polysaccharide and casein for potent curcumin delivery emulsions, *Food Chemistry* (2024), https://doi.org/10.1016/j.foodchem.2025.145045

Enhancing Emulsification and Encapsulation Stability *via* Maillard reaction of Garlic Polysaccharide and Casein for Potent Curcumin Delivery Emulsions

Xinyan Bai [a, b], Lingyu Li [a], X.G.Qiao [a], Wenqing Zhu [a, b], Yanna Hu [a], Laibing Sun [a], Marie-Laure Fauconnier [b], Zhenjia Zheng[a], and Yiteng Qiao[a, *],

[a] Key Laboratory of Food Nutrition and Healthy in Universities of Shandong, College of Food Science and Engineering, Shandong Agricultural University, 61 Daizong Street, Tai'an 271018, Shandong, P.R. China.

[b] Laboratory of Chemistry of Natural Molecules, Gembloux Agro-Bio Tech, University of Liège, Passage des déportés 2, B-5030, Gembloux, Belgium.

[*]Corresponding authors: Yiteng Qiao (Email: yitengqiao@sdau.edu.cn).

Abstract: Herein, the Maillard reaction between garlic polysaccharides (GPs) and casein (CN) was employed to enhance the emulsifying properties of CN. Structural characterization confirmed successful covalent conjugation, with a GPs/CN ratio of 1:2 at 70 °C and a grafting degree of 30.63%. Infrared and fluorescence spectroscopy demonstrated alterations in secondary and tertiary structures of CN following glycosylation. The introduction of hydroxyl groups increased the solubility of CN by 89.94%. The formation of C=N bonds and the disruption of crystalline regions further contributed to the improved emulsifying ability. Moreover, the emulsion achieved a curcumin encapsulation efficiency of 98.11%, with reduced particle size (343.93 nm to 242.65 nm) and Zeta potential (-38.14 mV to -14.33 mV). *In vitro* digestion showed that the induction of GPs into CN emulsion slowed the release rate of curcumin. This highlights the use of functional polysaccharides to modify proteins by Maillard reaction and create stable emulsion-based delivery systems.

Keywords: Garlic polysaccharide; Casein; Maillard; Delivery; Emulsion.

1. Introduction

Naturally sourced proteins are widely employed as emulsifiers, their capacity to stabilize emulsions and encapsulate hydrophobic bioactive compounds has rendered protein-based emulsions promising vehicles for functional ingredient delivery (Kim et al., 2020). Among these, casein (CN) has attracted particular interest due to its unique structural and interfacial properties. CN is a linear protein abundantly found in milk, and its flexible structure allows it to reduce interfacial tension more effectively than widely existing globular proteins, thereby exhibiting exceptional emulsifying capacity (Chen et al., 2024). However, its disordered and heat-insensitive structure limits its ability to form cohesive and irreversible interfacial films through thermal treatment. This structural deficiency results in relatively weak interfacial layers and compromises the long-term stability of casein-stabilized emulsions (Ma et al., 2021).

In recent years, the Maillard reaction has been increasingly applied to improve the functional properties of food proteins through conjugation with food-grade polysaccharides, without the need for chemical catalysts (Ai et al., 2021). This reaction can induce changes in protein structure, such as increased surface hydrophilicity, decreased α-helix content, and enhanced disordered (random coil) regions, which contribute to improved flexibility and interfacial adsorption. These structural changes are closely associated with enhanced emulsifying, foaming, and gelation behaviors (Cai et al., 2023). The emulsifying and foaming properties of xylo-oligosaccharides are significantly enhanced following their initial reaction with casein to produce Maillard products (Li et al., 2024). Furthermore, combining casein with dextrin can facilitate the preparation of an emulsion for lutein delivery (Liu et al., 2024). However, current studies have mostly focused on simple carbohydrates, and it remains unclear whether conjugation with bioactive polysaccharides through the Maillard reaction can yield comparable improvements in emulsification and delivery performance.

Garlic polysaccharide (GPs) is a major bioactive component of garlic with recognized antioxidant (Yan et al., 2021), modulates immunity (Wu et al., 2024),

anticancer (Kumari et al., 2022), and anti-aging activities (Bo et al., 2021). It possesses a (2 → 1)-linked β-D-Fruf backbone with (2 → 6)-linked β-D-Fruf branched chains and is resistant to degradation in the acidic environment of the stomach, enabling it to protect active compounds and promote their delivery to the intestine (Qiu et al., 2020; Qiu et al., 2024). Additionally, GPs possess terminal reducing carbonyl groups and free hydroxyl groups, which serve as effective reaction sites in the Maillard reaction. Their unique monosaccharide composition, such as the presence of galactose, also contributes to enhanced emulsifying properties after conjugation (Yang et al., 2023). It is reasonable to hypothesize that GPs participate in the Maillard reaction with CN, thereby facilitating the preparation of emulsions and enhancing the stability of casein emulsions, and this non-toxic conjugate has the potential to improve the delivery capabilities of emulsions. More importantly, their natural origin and multifunctionality align with modern consumers' demand for healthy and natural food products.

This study aims to investigate the Maillard reaction between GPs and CN to examine the effects of structural changes on emulsification properties, and to create a stable oil-in-water system with targeted delivery function potential for encapsulating lipophilic active substances. First, we prepared GPs-CN conjugates and characterized the structural changes of GPs-CN following the Maillard reaction. Subsequently, we explored how these structural changes affect emulsion interfacial properties. After obtaining a strong and stable emulsion, curcumin (a typical lipophilic active substance) was selected as the delivery object to explore the bioaccessibility during *in vitro* digestion. These findings offer novel insights into the enhancement of thermal and pH stability in protein emulsions, thereby improving the targeted delivery capabilities of multifunctional emulsions for lipophilic active substances.

2. Material and methods

2.1. Materials

The casein powder, which contains four casein subtypes, was isolated from milk and purchased from Beijing Solarbio Science & Technology Co., Ltd. (Beijing, China).

Vitamin E (VE, purity ≥ 99.0 %) was purchased from Fuji Oil Co., Ltd. (Osaka, Japan). Medium chain triglycerides (MCT, purity ≥ 99.0 %) were purchased from Caiwei Biotechnology Co., Ltd. (Jiangsu, China). Curcumin (Cur, purity ≥ 98.0 %) was from Shanghai Maikelin Biotechnology Co., Ltd. (Shanghai, China). Fluorescein isothiocyanate (FITC, 97 %, F6120) and Nile Red (95 %, N815046) were obtained from Macklin. All other chemicals were of analytical grade.

Garlic polysaccharides (GPs) were prepared from fresh garlic bulbs according to our previous study (Bai et al., 2022). The raw garlic is purple-peeled multi-clove garlic (purchased from Jinxiang County, Jining, China). The GPs were extracted with hot water and purified by removing protein and pectin (Bai et al., 2022). The extract was then purified by removing proteins and pectin. The purity of purified GPs was about 91.23%, and the extraction rate was 63.4%. Details of GPs were shown in **Table S1**.

2.2 Preparation of GPs-CN conjugates

GPs-CN conjugates were prepared via wet-heating according to the method of Zhang et al. (2022) and Zhang et al. (2022) with some modifications. GPs and casein were separately dissolved in distilled water at a concentration of 20 mg/mL. The solutions were then mixed at volume ratios of 6:1, 4:1, 2:1, 1:1, 1:2, 1:4, and 1:6 (*v/v*, GPs:CN), respectively. Each mixture was adjusted to a total solid concentration of 1.0 *wt*%, 1.5 *wt*%, or 2.0 *wt*%, and transferred into 50 mL centrifuge tubes. The samples were then incubated in a water bath at 60 °C, 70 °C, or 80 °C for 150 min to initiate the Maillard reaction. All samples were subsequently cooled to room temperature and stored at 4 °C for further analysis.

2.3 Emulsifying properties index

The emulsification activity index (EAI) and emulsion stability index (ESI) of the emulsions were determined according to the previously described method with some optimization (Kuang et al., 2023). CN and lyophilized GPs-CN conjugate samples were dissolved in UP water, and 35 mL of sample solution (1.0 *wt*%, 1.5 *wt*%, and 2.0 *wt*%) was mixed with 15 mL of oil phase. After pre-emulsification for 1 min, a high-pressure

homogenizer (SPX APV1000 High-pressure homogenizer, Germany) was used for homogenization at 800 Bar for 3 min. After emulsification for 0 and 3 min, the emulsion mixture was taken from the bottom of the bottle(50 μL), followed by diluting 100-fold with sodium dodecyl sulfate solution (0.1%, *w/v*). A_0 and A_3 were measured at a wavelength of 500 nm by a microplate reader (Thermo Multiskan GO, Thermo Scientific Ltd., USA). The EAI and ESI were calculated using the following Eq. 1 and 2.

$$\text{ESI (\%)} = \frac{A_0}{A_0 - A_3} \times 100\% \qquad \text{（Eq.1）}$$

$$\text{EAI (m}^2\text{/g)} = \frac{2 \times 2.303 \times A_0 \times n}{c \times (1-\varphi) \times 10^4} \times 10 \qquad \text{（Eq.2）}$$

Where *n* is the dilution factor, c is the concentration of sample solution (g/mL), φ is the oil fraction (*v/v*), and A_0 and A_3 are the absorbances of the emulsion at 0 and 3 min, respectively.

2.4 Characterization of the GPs-CN conjugates

2.4.1 Free amino acid determination

To determine the grafting degree of the Maillard conjugate products, the contents of free amino acids were detected by using the OPA (o-phthalaldehyde) method according to the previous study (Ajandouz et al., 2001). Firstly, 200 μL of the sample was mixed with 4.0 mL OPA solution, followed by the absorbance of the mixture was measured at 340 nm by the microplate reader (Thermo Multiskan GO, Thermo Scientific). The ultrapure water was a blank control. The degree of grafting (DG) of the original CN and the graft was calculated by Eq.3.

$$\text{DG (\%)} = \frac{A_0 - A_c}{A_0} \times 100 \qquad \text{(Eq.3)}$$

Where A_0 is the absorbance of CN, and *Ac* is the absorbance of the GPs-CN conjugate.

2.4.2 Solubility

The solubility of the samples was measured using the method described by Nooshkam et al. (2022) with slight modifications. Briefly, the samples were first

dispersed in water (2.0 mg/mL protein content) at pH 7. The solution was centrifuged for 15 min at 7,000 rpm, take the supernatant (1 mL) and Biuret reagent (4 mL) was added. The absorbance of the supernatant was measured at 540 nm using a microplate reader (Thermo Multiskan GO, Thermo Scientific) after 20 min of reaction. Solubility was calculated based on the Eq.4.

$$\text{Solubility (\%)}=\frac{C_1}{C_0}\times 100\% \qquad \text{(Eq.4)}$$

Where C_1 is the CN concentration in the supernatant, and C_0 is the CN concentration in the initial sample.

2.4.3 Fourier transform infrared (FTIR) and Circular dichroism(CD) analysis

FTIR and CD analyses were performed as previously reported (Wang et al., 2023). The freeze-dried GPs-CN was measured by a Thermo Nicolet IS10 FTIR spectrometer (Thermo Fisher Scientific Inc., USA) and J-1500 circular dichroism spectrometer (JASCO Ltd., Tokyo, Japan). All samples (3.0 mg) were measured using a Thermo Nicolet IS10 FTIR spectrometer (Thermo Fisher Scientific Inc., USA), scanned 64 times in the wavenumber range of 4000 cm^{-1} to 400 cm^{-1} at a resolution of 4 cm^{-1}(Fauziee et al., 2021). The CD analysis was performed using the protocol described by Nan et al. (2020). Quartz cuvette was placed in a J-1500 circular dichroite spectrometer (JASCO Ltd., Tokyo, Japan). The optical diameter of the sample cell is 1 cm, the step size is 0.1 nm, the scanning range is 190–250 nm, and the scanning speed is 120 nm/min.

2.4.4 Fluorescence analysis

Fluorescence spectral changes in individual lyophilized samples were determined with a fluorescence spectrophotometer (Lumina, Amarica Thermo Ltd., Waltham, USA). The parameters were set according to the previous method (Yin et al., 2023). The emission spectrum is 300–500 nm, the excitation and emission slit width were set as 5 nm at the voltage of 420 V.

2.4.5 UV-Vis wavelength scanning

The UV-Vis absorption spectrum of the samples was analyzed using the UV-Vis full-wavelength scanning method for proteins by Lei et al. (2023), and the absorption spectrum from 220 to 400 nm was measured using a UV-2450 spectrophotometer (Shimadzu Ltd, Kunshan, China).

2.4.6 X-ray diffraction (XRD) analysis

XRD analysis was employed to investigate the crystalline structure, with modifications made based on a previously reported method (Wang et al., 2023). The parameters were evaluated using an XRD ray diffractometer (D8-Advance, German Bruker Ltd., Germany) at 40 kV and 40 mA in reflection mode. According to the test results, the scanning was carried out between 5° and 90° (2θ), with a step size of 0.02° and a scanning speed of 30°/min.

2.4.7 Three-phase contact angle test

A contact angle meter (DSA100S, KRÜSS, Germany) was used to determine the three-phase contact angle of samples as reported (Wang et al., 2023). The treated sample was placed in a corn oil glass tank purified by Florisi adsorbent and put on the stage. Ultrapure water was dripped onto the sample disc using a high-precision syringe. After stabilization for 30 s, the surface morphology of the disc was photographed with a high-speed camera. The Laplace-YOUNG equation was used to simulate the imaging droplet profile to obtain the hydrophilic oil state of the sample.

2.5 Preparation of GC emulsion

The emulsion was prepared following the modified method of Xu et al. (2017) with slight modifications. Initially, a casein-based water phase and water phase containing GPs-CN conjugates were prepared at concentrations of 1.0 wt%, 1.5 wt%, and 2.0 wt%. The oil phase was composed of a medium-chain triglyceride (MCT) and vitamin E (VE) mixture in a 1:1 (*v/v*) ratio. The water phase and oil phase were then mixed at a 3:7 (*v/v*) ratio, and pre-emulsified using a magnetic stirrer for 10 min. The resulting mixture was homogenized using a high-pressure homogenizer (SPX APV1000, Germany) at 800 Bar for 3 min to achieve uniform particle size distribution.

To prevent microbial growth, sodium azide (NaN_3) solution was added to the emulsion at a concentration of 0.02% (*w/w*).

2.6 TEM and CLSM analyses

The microscopic observation methods of the samples were all based on the methods of previous studies, and the details were fine-tuned according to the field of view during the observation process (Wang et al., 2023). The morphology of the emulsion was characterized by a Transmission Electron Microscope (TEM) (Hitachi HT7800, Tokyo Ltd, Japan). All samples were diluted 100-fold with ultrapure water, followed by 10 μL of diluted emulsion was dropped onto a copper grid with a formvar membrane. After drying, the samples were observed at an accelerating voltage of 80.0 kV.

Confocal laser scanning microscopy (CLSM) was used to reveal the interfacial structure of the emulsion droplets. The emulsions were inspected with a confocal laser scanning microscope (LSM 880, Carl Zeiss, Gottingen, Germany). Nile Red (1.0 mg/mL) and FITC (1.0 mg/mL) were used to stain the oil phase and aqueous phase of the emulsion. Nile red was excited at a wavelength of 488 nm and emits fluorescence in the 570–600 nm range, while FITC is also excited at 488 nm but emits at a wavelength of 525 nm.

2.7 Rheological properties

The rheological behavior of the emulsions was tested according to the method of Spotti et al. (2019) using a modular compact rheometer (MCR102, Anton Paar GmbH, Austria). A plate with a diameter of 40 mm was used and the sample gap was set to 1,000 μm. First, a dynamic scanning test was performed, and a strain scanning test with a frequency of 1 Hz was performed, and the strain range was from 0.1% to 100%. This is followed by a steady-state shear scan to measure the shear viscosity at different shear rates, ranging from 1 to 100 s^{-1}. All the above measurements were carried out at 25 °C. Finally, the storage modulus (G′) and loss modulus (G″) of the sample were recorded

in the heating rate range of 25 to 90°C to test the rheological properties of the emulsion during the thermal change process.

2.8 Low-field nuclear magnetic resonance (LF-NMR) analysis

T_2 relaxation time was measured by LF-NMR spectrometry according to the method by Zhao et al. (2023). The main frequency was 21 MHz, the RF delay was 0.002 ms, and the echo time was 0.4 ms with a LF-NMR Analyzer Benchtop NMR MicroMR02-025V (Niumag Co., Jiangsu, China). In a predetermined 100,000 echoes, a multi-exponential fitting curve is applied to fit the attenuation curve. The Carr-Purcell-Meiboom-Gill (CPMG) pulse sequence was utilized. D_2O was used instead of water in the emulsion for deprotonation.

2.9 Preparation of emulsions for delivery of curcumin

Following the method described by Xu et al. (2017) with slight modifications, curcumin was first completely dissolved in absolute ethanol to prepare a stock solution at a concentration of 10.0 mg/mL. An appropriate volume of the curcumin-ethanol solution was then added dropwise into the aqueous phase containing GPs and CN, with a maintained GPs:CN mass ratio of 1:2 (*w/w*), under continuous stirring to ensure homogeneity. The aqueous phase was subsequently mixed with the oil phase at a water-to-oil ratio of 1:4 (*v/v*) to form a pre-emulsion. The emulsion was then subjected to high-pressure homogenization under the conditions described in **Section 2.5**.

2.9.1 Determination of encapsulation ability

The maximum encapsulation efficiency (LE) and drug loading capacity (LC) of curcumin were determined using the centrifugation method (Yang et al., 2020; Sun et al., 2024). The emulsion sample was centrifuged at 8000 × g for 10 min to remove unencapsulated insoluble curcumin, and the supernatant was diluted in absolute ethanol. The absorbance of the sample was then measured using a UV-Vis spectrophotometer at a wavelength of 420 nm. The curcumin content in the emulsion was calculated based on the LE and LC of the emulsion using Eq.5 and Eq.6.

$$\text{LE}（\%）= \frac{M_{CL}}{M_C} \times 100\% \qquad \text{(Eq.5)}$$

$$\text{LC（\%）} = \frac{M_{CL}}{M_{TM}} \times 100\% \qquad \text{(Eq.6)}$$

Where M_{CL} was the mass of curcumin loaded in the emulsion; M_C was the initial mass of curcumin in the system; and M_{TM} was the total mass of curcumin nanoemulsion (Cur, GPs and CN).

2.9.2 Effects of temperature and pH value on rheological properties of emulsions

The constant strain was 0.05% (a condition obtained by previous static viscoelasticity tests) and was tested according to previous studies (Shen et al., 2017). The apparent viscosity (η) of the emulsion should be measured in the shear rate range of 0.1 to 1000 s^{-1}.

2.9.3 Size and Potential (PDI) characteristics of emulsion

The size, PDI, and zeta potential of all samples were determined by a Zetasizer Nano-ZS90 (Malvern Instruments, Worcestershire Ltd, UK). To ensure data consistency, all samples were diluted 100-fold with ultrapure (UP) water and equilibrated at 25 °C for 2 min.

2.9.4 Stability verification of curcumin emulsions

The stability of emulsions was tested with the Turbiscan LAB (Microtrac MRB, Verder Scientific Ltd, France). The sample was transferred into a small 5.5 mL sample cell, followed by measurement at 25 °C for 10 h (Yang et.al, 2021).

2.9.5 *In vitro* simulation of bioaccessibility

A modified version of a previously reported method was used to measure the *in vitro* release of curcumin from emulsions (Li et al., 2024). An environment simulating gastrointestinal digestion *in vitro* was prepared. Pepsin (30 mg, 2000 U/mL) was dissolved in 10 mL of saline, and the pH was adjusted to 1.2 to obtain simulated gastric fluid (SGF). Simulated intestinal fluid (SIF) and simulated colon fluid (SCF) were prepared by dissolving 100 mg of porcine bile salts, *β*-glycanase(50 U/mL), and trypsin (30 mg, 100 U/mL) in 10 mL of phosphate buffer, adjusting the pH to 6.8 and 7.4 with 7.0 M NaOH, respectively. The simulated digestion process involved dispersing the curcumin-encapsulated emulsion in simulated gastric juice, stirring at 37°C. Samples

were collected per hour, and curcumin content in the supernatant was determined after centrifugation (4,000 ×g, 15 min). After 3 h, an equal volume of simulated intestinal fluid was added to the digestive juice and stirred. Samples were collected per hour and centrifuged for measurement. Finally, the mixture was digested in simulated colon fluid and stirred for 6 h, and Cur content was measured per hour.

2.10 Statistical analysis

All experimental results were determined in triplicate and expressed a mean ± standard deviation (SD). One-way ANOVA and Duncan's comparison tests were used for statistical analysis using SPSS statistical software at $p < 0.05$.

3. Results and discussion

3.1 Specific structure and characteristics of GPs-CN

3.1.1 Emulsification Indicators of GPs-CN

The EAI and ESI were measured at different temperatures (60–80 °C) and different pH values (pH 7 and pH 4), and the GPs:CN ratio (6:1, 4:1, 2:1, 1:1, 1:2, 1:4, 1:6, *v/v*) (**Fig. 1(A, B, D, E) and Fig. S1**). The ESI and EAI can be used for reflecting the emulsification properties of emulsions (Zhang et al., 2022). The ESI and EAI of glycated protein increased at 60 °C and 70 °C, and there was a significant difference ($P < 0.05$) (**Fig. S1 A~D**). In addition, the ESI variation range at 80 °C was unstable in the range of 3.37–9.83 m^2/g (**Fig. S1 E~H**), further glycation reduces the surface hydrophobicity of SPI, disrupts the balance between its hydrophilic and hydrophobic properties, and impairs its interfacial adsorption ability, ultimately leading to a decrease in emulsification efficiency (Cui et al., 2023). Therefore, in the subsequent emulsion preparation study, the glycosylation reaction was stably controlled at 70 °C.

As shown in **Fig.1D** and **E**, the ESI and EAI indices of GPs-CN conjugates were significantly improved compared with CN ($p < 0.05$). The ESI and EAI were increased by 8.1% and 6.2 m^2/g at a GPs:CN ratio of 1:2 (*v/v*) at pH 7, and positively increased with the increasing GPs concentration. In addition, the ESI and EAI values of the emulsions were prepared by different glycosylation concentrations (1.0 *wt*% to 2.0 *wt*%

of the water phase) were significantly different ($p < 0.05$), which showed that GPs may co-adsorb with GPs-CN at the oil-water interface, improving the uniformity and strength of the interfacial layer. The appropriate concentration of conjugates as a surfactant was uniformly distributed on the oil-water interface, reducing the surface tension and improving the emulsification potential. Hydrophilic polysaccharides can increase the thickness and flexibility of the oil-water interfacial film, thereby improving emulsion stability (Etale et al., 2023). Therefore, the addition of 1.5 *wt*% GPs-CN results in the formation of conjugates with strong emulsifying properties at pH 7.

3.1.2 Detection of grafting degree(DG)

Table 1 Grafting and solubility of glycosylates under different conditions

Sample	DG (%)	Solubility (%)
CN	0	-
GPs:CN (6:1)	10.26±1.02*	78.94±2.19**
GPs:CN (4:1)	11.74±1.34*	76.33±1.88**
GPs:CN (2:1)	13.26±1.29*	87.29±1.59**
GPs:CN (1:1)	26.68±2.10**	88.83±2.08**
GPs:CN (1:2)	30.63±1.22**	89.94±1.90**
GPs:CN (1:4)	28.36±1.35**	76.43±2.26**
GPs:CN (1:6)	26.74±1.29**	71.44±1.78**

- means extremely poor solubility, causing deviation in the measurement of grafting degree. Compared with CN at a significant level *$p < 0.05$; **$p < 0.01$

The GPs and CN were used to produce different grafting degrees at pH = 7. As shown in **Table 1**, the grafting degree was the minimum of 10.26 ± 1.02% at a GPs:CN ratio of 6:1, and the solubility of the graft was significantly improved ($p < 0.01$) compared with the solubility of the original casein, indicating that glycated modification by Maillard effectively improved the solubility of CN. With the increase of the CN ratio, the DG of the conjugate was gradually increased until 30.63 ± 1.22% at a GPs:CN ratio of 1:2, and the solubility was significantly improved ($p < 0.01$), which

was about 10% higher than CN. This result was caused by the different solubility of the conjugates, and other properties of the material may also be affected (Yao et al., 2023). It was noticed that the solubility of the graft was 76.43 ± 2.26% and 71.44 ± 1.78% at a GPs:CN ratio of 1:4 and 1:6, they were not increased with the grafting degree. This may be due to the excessive interaction between polysaccharides and casein, which inhibits the dissociation of protein micelles (Ding et al., 2021).

3.1.3 FT-IR spectroscopy

Fig. 1 ESI and EAI of the GPs:CN ratios ranged at pH 7(A, B), pH 4.6(D, E) at 70 °C; FT-IR(C), Fluorescence(F) of the GPs:CN = 6:1, 4:1, 2:1, 1:1, 1:2, 1:4, 1:6

FT-IR is effective in detecting the interaction between proteins and polysaccharides at the molecular level after the Maillard reaction (Liu et al., 2024). As shown in **Fig. 1C**, it can be seen that the biggest difference between the conjugate and CN was in the amide I (1600–1700 cm^{-1}) and II amide (1500–1600 cm^{-1}). The bands at 1669 and 1560 cm^{-1} correspond to amide I and amide II of CN, respectively. Compared with the CN, the amide II band of each GPs-CN conjugate showed a higher intensity absorption peak, this change may be due to the appearance of new functional groups caused by the Maillard reaction, such as the C=N of Schiff base, the C=O of Amadori product and the C–N functional group of Heyns (Qu et al., 2021). The covalent bonds of these amino and carbonyl groups enable GPs-CN conjugates to adsorb at the oil-water interface to form a compact and thick film, thus affecting the emulsification ability of glycosylated products.

In addition, the absorption of GPs-CN conjugate in the 1050-950 cm^{-1} region was stronger than that of CN, which corresponds to the side chain vibration of the protein (Chang & Tanaka, 2002). The GPs-CN conjugate peaks at 1079 cm^{-1} and 3338 cm^{-1} showed more significant enhancement than those of the CN conjugate peaks. The increased absorption intensity in the wavelength range of 1000–1260 and 3000–3700 cm^{-1} is due to C–O and O–H stretching vibrations, which proves the formation of Maillard reaction products in proteins and polysaccharides (Liu et al., 2024), and the

introduction of –OH groups also increase the hydrophilicity of CN, thereby improving the emulsification properties. In addition, the C–H peak at 2970 cm^{-1} was also enhanced, which helped to improve the interfacial adsorption capacity of GPs-CN (Saw et al., 2023).

3.1.4 Fluorescence analysis

As can be seen in **Fig. 1F**, the fluorescence signal of casein was the most obvious, and the fluorescence intensity of the grafted products was reduced compared with casein. Tryptophan can often be used as an endogenous fluorescent probe in Casein. The fluorescence signal of tryptophan can be effectively blocked by the occurrence of glycosylation reaction (Verma et al., 2023). It was worth noting that when the GPs:CN ratio was 1:2, 1:4, 1:6, 1:1, 2:1, 4:1 and 6:1, the DG values of the grafted products decreased stepwise. As the concentration of CN increases, the Maillard reaction gradually becomes stronger until the ratio of GPs to CN reaches 1:2. There may be a steric hindrance effect, which makes the Maillard reaction no longer violent (Yan et al., 2022). As the degree of grafting increases, the maximum fluorescence intensity gradually decreases (**Fig. S3**), indicating that the maximum fluorescence intensity was linearly related to the degree of grafting. When GPs were grafted on CN, the fluorescence signal of tryptophan on CN was shielded and the fluorescence intensity was reduced.

3.1.5 UV absorption spectral variability

As shown in **Fig. S2B**, after the initial Maillard reaction between polysaccharides and proteins, the characteristic peaks of the UV band were possessed by the products of specific Schiff base secondary structures, which caused the UV characteristic peaks of proteins to be red-shifted (Jiang et al., 2023). When the ratio of GPs:CN changed and different degrees of grafts were generated, the UV absorbance of these grafts changed to different degrees, and they all showed characteristic broad peaks. The changes in the number of representative groups such as amino and carbonyl groups in different grafts cause changes in the intensity of the UV absorption peak. When the maximum

absorption value of the broad peak at a GPs:CN ratio of 1:2 was shifted from the 281 nm red shift of the broad peak at CN to the 292 nm, which was similar peak properties to Dong et al. (2019) in the preparation of emulsions from Maillard products of flaxseed gum and whey protein isolate, and these structural changes were covalent additions, which may affect the self-associative properties of casein micelles and thus their emulsifying properties.

3.1.6 CD analysis

Circular dichroism spectrometry analysis further elucidated the extent of changes in the secondary structure of glycosylation products (**Fig. S2 A**). A prominent negative peak is observed in the range of 200–210 nm, with the characteristic peak at 208 nm corresponding to α-helix, while the peak at 200 nm represents disordered coil; notably, these two peaks exhibit overlapping characteristics. Beyond a wavelength of 206 nm, the peak bands of all GPs-CN conjugates begin to shift towards the positive peak direction, which is attributed to the characteristic peak band of the *β*-chain (Hohmann et al., 2023). This observation indicates that all conjugates contain numerous *β*-turns and random coils.

We used *DichroWeb* software to analyze the relative percentage content of each secondary structure of the samples. As shown in **Table S2**, the GPs-CN conjugates were dominated by the *β*-Strand structure, followed by *β*-Turns and *α*-Helix structures. In addition, under a mass ratio of 1:2, the structural ratio in GPs-CN changed significantly ($p < 0.05$) compared to CN. In comparison to the original CN, the *β*-strand was reduced by 3.84%, while the *β*-turns measured 12.10 ± 0.05%. The reduction of the *β*- strand and *β*- turns may decrease the precipitation or micronization of aggregates, thereby enhancing the effective concentration of the emulsifier (Zhao et al., 2024). The disordered configuration ratio significantly increased ($p < 0.05$) by 37.79 ± 0.27%, indicating that the Maillard reaction between CN and GPs was optimal at a GPs:CN ratio of 1:2. Similar changes were observed in the preparation of whey protein and xylose grafts (Shang et al., 2020). The elevated proportion of disordered regions

enhances the molecular flexibility and hydrophilicity of the conjugates, enabling them to rapidly adsorb to the oil–water interface. This facilitates the formation of a dense interfacial layer, improving emulsification efficiency and enhancing the physical stability of the emulsion system (Zhang et al., 2022).

3.1.7 XRD analysis

Fig. 2 XRD of the GPs∶CN ratios ranged from different samples

The XRD analysis of CN and GPs-CN was shown in **Fig. 2**. As can be seen from **Fig. 2**, the strong peaks of all glycosylation products at 20 ° shifted to the left to varying degrees, and the original sharp peak of CN at 8 ° disappeared, indicating that C=N and C=O bonds formed between the CN and GPs caused changes in the secondary structure, leading to the transformation of the original α-helix and β-sheet structures into random coils, thereby weakening the crystal structure to varying degrees. A broad diffraction peak appeared when the GPs:CN ratio was 1:2, and there was also a broad diffraction peak at 2θ=30 °–40 °, which was a manifestation of reduced crystallinity. The flexible interfacial film of low-crystallinity emulsifiers can effectively inhibit the aggregation of emulsion droplets in the emulsion and enhance the long-term stability of the emulsion (Song et al., 2024). The crystal structure of CN can be altered by the Maillard reaction with GPs. This weakening of the crystal structure may be necessary to optimize the interfacial behavior of CN.

3.1.8 Hydrophilic and lipophilic nature of the GPs-CN conjugates

Fig. 3 Contact angle the CN(A) and at the GPs∶CN ratios of 6∶1(B), 4:1(C), 2:1(D), 1:1(E), 1:2(F), 1:4(G), 1:6(H) at pH 7

The amphiphilicity of the emulsifier is closely related to the radius of the particles, oil-water interfacial tension, three-phase contact angle, the type and concentration of counterions, and temperature (Aronson et al., 1980; Rezvani et al. 2024). As shown in **Fig. 3** (**A, B, C, D**), the contact angles when the GPs∶CN ratios were 6:1, 4:1, and 2:1 were 57.19 °, 69.35 °, and 76.67 °, respectively. As the proportion of CN in the GPs-CN conjugates was increased, the contact angle was increased. Compared with CN, the

contact angle was increased by 31.5 °at the GPs:CN ratio of 1:2(**Fig. 3F**). The reason for the increase was that the contact angle was in the range of 0–90 °, the material had strong hydrophilicity, a little energy was required by the particles to cross the interface into the water phase, most of the surface area of the particles was dispersed in the water phase, and it was easy to form an oil-in-water system (Meng et al., 2023). When the mass ratio of GP to CN was 1:1 and 1:4, the contact angle was 90.89 ° and 100.83 °(**Fig. 3E&G**). The sample had good lipophilicity when the contact angle was > 90°, and the closer the contact angle was to 180 °, the water-in-oil system was easily formed (Gowthami et al., 2023; Li et al., 2024). Especially, the contact angle of the GPs-CN conjugates was 100.12 ° at the ratio GPs:CN was 1:6 (**Fig. 3H**), indicating the complex exhibited good lipophilicity. In general, the GPs-CN conjugates had good emulsification properties and controllability compared with CN.

3.2 The PDI and particle size of emulsions

Different conjugates have different effects on the aggregation of droplets (Kuang et al., 2023). As shown in **Fig. 6A**, when the GPs-CN conjugates were distributed on the water surface as a droplet stabilizer, the Zeta potential of the emulsion was fixed at the oil phase fraction, and the size of the generated oil droplets changed with the emulsification properties of the conjugate. The hydrophilicity of proteins can be enhanced due to the increased degree of glycosylation, and the hydrophilic groups of polysaccharides are introduced (Wu et al., 2020). The absolute value of the Zeta potential of the G1C2 emulsion was significantly increased ($p < 0.05$) compared with the casein-stabilized emulsion, reaching a maximum value of 39.85 ± 1.20 mV. At this time, the outside of the emulsion droplets was covered with negative charges, and there was a huge repulsion between the droplets. **Fig. 6B** showed that although the glycosylation effect in the G6C1 emulsion was not significantly exerted, it also had a significantly ($p < 0.05$) smaller particle size (261.7 ± 0.4 nm). This may be because the oil droplets were stabilized in the excessively high concentration of GPs water phase. The average particle size of the G1C2 emulsion had correspondingly reached a

minimum value of 240.4 ± 1.4 nm, indicating that the displacement force of the emulsion droplets was the strongest at this time, and the G1C2 emulsion can be used as a stable emulsion.

3.3 TEM analysis

Fig. 4. TEM image of CN emulsion(A), G6C1 emulsion(B), G4C1 emulsion(C), G2C1 emulsion(D), G1C1 emulsion(E), G1C2 emulsion(F), G1C4 emulsion(G) and G1C6 emulsion(H)

The morphology and size of individual latex particles can be observed by TEM. The droplets of latex in water were spherical with a light outer shell (Li et al, 2021). As shown in **Fig. 4**, the latex particles produced by different grafting were presented in the TEM images. The droplets with diameters of 580.88 nm, 683.82 nm, 580.90 nm, 518.38 nm, 893.38 nm, 485.29 nm, 580.88 nm, 606.61 nm were captured by CN, G6C1, G4C1, G2C1, G1C1, G1C2, G1C4 and G1C6 emulsion, respectively. The total particle size of all O/W emulsions was the smallest at 485.29 nm, and the shell thickness was 91.91 nm at a GPs:CN ratio of 1:2, the particle size of the emulsion formed by a single CN was 580.88 nm, while the shell of the G1C2 emulsion was thinner than the CN emulsion, accounting for only 18.93% of the total particle size of the oil droplet. Therefore, the TEM image results of the oil droplets were similar to the results of the particle size analysis.

3.4 Emulsion rheological characteristics

Fig. 5 (A) Changes in the storage modulus during heating from 25°C–90 °C; (B) The Compound viscosity in different temperatures; (C) LF-NMR for emulsions; (D) The energy Loss modulus during heating from 25°C–90°C; (E) Apparent viscosity and stress as a function of shear rate for emulsions; (F) Details in LF-NMR for emulsions

As shown in **Fig. 5A**, the G′ value of each grafted emulsion was increased as the temperature was increased. The reason for the increase was that the oil droplets in each emulsion accelerated. Generally speaking, heat treatment conditions often lead to protein denaturation and aggregation, such as decomposition and folding, which affects

the emulsification effect of protein emulsifiers in stable emulsions (Farjami et al., 2021). The thermal stability of the emulsion was prepared by GPs grafted CN was higher than the CN emulsion, and the proportion of polysaccharides in glycosylation was concentration-dependent. In **Fig. 5D**, the G″ value of all emulsions was significantly increased by glycosylation, similar to the change of the G′ value. The inflection points of temperature were statistically shown in **Fig. S4**. The inflection point of the G1C2 emulsion was 89.25 °C, and the CN emulsion was 75.22 °C. This change showed that the loss modulus of the emulsion was increased with increasing temperature. This may be because the non-polar groups wrap around the protein by Maillard reaction, to prevent changes in protein thermal (Lu et al., 2024). Generally, the thermal sensitivity of the G1C2 emulsion was the most obviously reduced, and the emulsion had superior damping performance.

As shown in **Fig. 5B**, the hot melt properties of the emulsion reflected on the increasing composite viscosity of the emulsion as the temperature gradually. Solubilizers were often used in hot melt emulsions to disperse and transport active substances with high thermal efficiency and poor solubility, such as flavonoids, which can be improved the water solubility and utilization rate (Dadwal et al., 2023). The melting curve of the G1C2 emulsion was raised slowly, and the G1C2 emulsion had good thermal stability. We further explored the shear viscosity/shear stress of emulsions of shear rate was shown in **Fig.5E**.With the Shear rate was increased, emulsions exhibited similar flow curves with the shear viscosity in the range of 0–10 mPa.s. While the difference in Shear stress could be redounded to the emulsion properties (Yang et al., 2021)

3.5 Low-field nuclear magnetic resonance (LF-NMR) analysis

LF-NMR analysis can provide insights into the behavior of the water and oil phases in a flowing state, while also confirming that the emulsion remains intact (Wang et al., 2022). As shown in **Fig. 5C** and **Fig. 5F**, the G1C2 emulsion was significantly differed from the other emulsions. The relaxation time curve has four peaks, of which

two peaks are in the T_{21} value. The peaks in the T_{21} range indicate that the water phase in the G1C2 emulsion sample was bound with a strong binding force. While three peaks except for the G1C2 emulsion were shown by the relaxation time curves of all emulsions. T_{21} (about 0.1–10 ms) was the region where the bound water signal peak was detected, T_{22} needs to be observed for the changes in the LF-NMR signal curve within the range of about 10–100 ms, the migration level of nonflowing water indicated the range, and T_{23} was repressed the migration of free water within the range of 100–1000 ms. These emulsions were complex systems with high viscosity, the high content of hydrophobic groups allows the macromolecules to cross-link to form a dense network, and the oil droplets move slowly, thereby achieving rapid diffusion and adsorption at the oil-water interface, forming a stable interface layer (Ribeiro et al., 2012; Lin et al., 2023). In summary, the T_{21} of different graft emulsions was decreased to varying degrees compared with the CN emulsion. This decrease was due to the change in protein structure caused by glycosylation, which led to changes in protein hydrophilicity. The unstable properties of casein raw emulsion were changed by the glycosylation reaction caused by adding polysaccharides.

3.6 Delivery of curcumin using stable G1C2 emulsion

In recent years, due to the high hydrophobicity of curcumin, relevant studies on its delivery using O/W emulsions have emerged. The encapsulation and release behavior of curcumin largely depend on the physicochemical properties of the carrier system (e.g., droplet size, interfacial composition, and pH value), making it an effective probe for evaluating the performance of emulsion formulations (Kara et al., 2024). Curcumin (Cur) was dissolved in MCT + VE containing 10% ethanol (*v/v*) to increase the solubility of Cur in the oil phase (Salehi, 2014). We used an optimized G1C2 emulsion as a loading and delivery system and compared the drug loading and encapsulation rates with the casein-based emulsions. The CLSM images of the G1C2@C and CN@C emulsions were shown in **Fig. S5**. Both emulsions exhibited a well-defined capsule shell structure, with the water phase outside the shell and the oil phase inside. This

structure was consistent with findings from Wang et al. (2023). The droplet size of the G1C2@C emulsion was more uniform compared to that of the CN@C emulsion.

3.6.1 Delivery rate of encapsulated curcumin

Fig.6 Average particle size and PDI (A), and zeta potential (B) of CN and GPs-CN conjugates; Drug LC (C) and LE (D) at Different addition amounts of curcumin emulsion**;** Particle size potential and zeta potential of CN@Cur emulsion and G1C2@Cur emulsion at different temperatures (E) and pH (F). Different letters mean values showed significant differences ($p < 0.05$).

As shown in **Fig. 6 (C, D)**, both the drug loading rate and the encapsulation rate were changed with the addition of Cur. The LE of G1C2@Cur emulsion was significantly higher than CN@Cur, with LE of 98.11 ± 0.74% and LC of 43.97 ± 0.45%. Compared with the optimal LE (95.93 ± 0.5%) of CN@Cur emulsion, the LE of G1C2@Cur emulsion is improved by 2.17%. In addition, with the addition of Cur, the LE was not increased significantly ($p > 0.05$), and the LE was optimal at 10% (*w/w*), which may be related to the solubility of Cur in the oil phase. Therefore, CN@Cur emulsion and G1C2@Cur emulsion with an additional amount of 10% were used as the objects of subsequent research.

3.6.2 Thermal stability of curcumin emulsions

Emulsions were thermodynamically unstable systems and must be stabilized by surfactants. As shown in **Fig. 6E**, as the temperature increased, the particle size of the CN@Cur emulsion was increased continuously and showed a linear upward trend. The reason for the increase in particle size was that the Collision velocity between the casein-based emulsion droplets in the CN@Cur emulsion was changed from 30°C to 80 °C. With the increase in temperature, droplet aggregation occurs to varying degrees. The particle size of the G1C2@Cur emulsion did not be changed significantly ($p > 0.05$) within the tested temperature range, and the particle size ranged from 217.1 ± 0.3 nm to 238.9 ± 0.3 nm, but the particle size of the emulsion gradually decreased at > 60 °C, which was opposite to the original CN@Cur emulsion. Similar results were also found

in the previous study of Mo et al. (2022). This result indicated that the CN structure was changed, which may be led by the glycosylation reaction of GPs and CN. When the polysaccharide chains were contained in the appropriate proportion were fully extended in the aqueous phase, and the high-speed moving droplets at high temperatures were protected by the thick micelle shell formed, which the thermodynamic properties of the protein can be stabilized (Li et al., 2022).

As shown in **Fig. 7A**, a decreasing trend was presented with the increase in shear rate, which was an inevitable characteristic of non-Newtonian fluids (Li et al., 2022). In the range of 30–80 °C, the apparent viscosity of G1C2@Cur emulsion was higher than that of CN@Cur emulsion. This high viscosity increased the stability of the emulsion system, which corresponded to the particle size and surface charge determination of the samples.

3.6.3 pH stability of curcumin emulsions

The Zeta potential of CN@Cur emulsion and G1C2@Cur emulsion were decreased with the increase of system pH (**Fig. 6F**). The negative charge on the surface of all emulsion droplets was overloaded from pH > 4, and the Zeta potential of the entire emulsion system was negative. Moreover, the electronegativity of G1C2@Cur emulsion has electronegativity at the isoelectric point of casein, indicating that the adsorption properties of the original casein micelles were changed by glycosides to the environmental charge, thereby isoelectric point was changed, which was similar to the properties of the Maillard reaction products of whey protein and dextrin (Pan et al., 2019). In addition, a trend of gradually increasing particle size was presented with increasing pH, and the particle size of CN@Cur emulsion and G1C2@Cur emulsion gradually stabilized when pH > 5, indicating that these two curcumin emulsions may be in a relatively stable O/W emulsified droplet state under weakly acidic and alkaline conditions.

Fig. 7C showed the morphology of CN@Cur emulsion (C(a)) and G1C2@Cur emulsion (C(b)) under different pH conditions. CN@Cur emulsion produces floccules

at pH 4 and 5, while G1C2@Cur emulsion was unstable only at pH 4. As shown in **Fig. 7B**, the rheological properties of different emulsion samples were in the pH 2–9. The viscosity of the emulsion continuous phase and the adsorption of polymers at the oil-water interface were the keys to stabilizing the oil-in-water system. When the pH of the emulsion was lower than the pI of CN(pH = 2–4), due to the deprotonation of G1C2, the G1C2@Cur emulsion exhibited high viscosity behavior, and the degree of flocculation was increased. Similar to previous studies on xanthan gum-whey protein emulsions (Sriprablom et al., 2019), the viscosity of the emulsion was decreased with the shear rate was increased at pH 5–9.

3.6.4 Emulsion stability

Fig. 7 Viscosity of CN@Cur emulsion and G1C2@Cur at different temperatures (A) and different pH (B); appearance photograph of the emulsions stabilized by CN@Cur (C(a)) and G1C2@Cur (C(b)) with different pH; TSI, T and BS spectra of CN@Cur (D(a))and G1C2@Cur(D(b)) emulsions for 24 h. Insert photographs of emulsions after 15 h.

The use of Turbiscan LAB technology to evaluate the stability of emulsions is a short and effective method. The sample is irradiated with a near-infrared light source, and then the background scattering is collected and the signal is transmitted from the bottom to the top of the sample at the full height(Wang et al., 2022). As shown in **Fig. 7D(a)**, the higher TSI value means the less stable system. The TSI index of the G1C2@Cur emulsion was significantly better than that of the CN@Cur emulsion, the reason may be compared with CN, GPs-CN conjugates produced a thick interfacial layer and a high absolute value of zeta potential inside the emulsion, the running speed of the emulsion oil droplets was slowed down, and the stability of the emulsion was increased.

Fig. 7D(b) showed the BS curve and T curve of the emulsion stored for 15 h. The change of the BS curve directly represents the movement of the oil droplets in the system. The decrease on the left side of the BS curve indicates the decrease in the oil

droplet concentration and clarity at the bottom of the system, and the increase on the right side of the BS curve indicated that the ridge layer was enlarged with time (Gao et al., 2022). The left side of the BS curve of the CN@Cur emulsion decreased with time, indicating that the bottom of the system gradually became clear and the oil droplet concentration decreased. The CN@Cur emulsion was not stabilized due to coagulation or flocculation after 7 h. The BS curve of the G1C2@Cur emulsion was showed a stable trend, and the backscattered light intensity was showed an upward trend after 13.5 h. The reason for the increase was that the movement mode and movement speed of the droplets in the G1C2@Cur emulsion system were different from those of the CN@Cur emulsion. It was further demonstrated that the glycosylation of GPs and CN altered the emulsifying ability of CN, and Cur could be stably encapsulated in the G1C2@Cur emulsion, which was an effective means for efficient delivery of Cur.

3.6.5 In vitro digestion characteristics of G1C2@Cur emulsion

Fig. 8 The distribution state of the droplets and droplet size of G1C2@C in different digestive fluids(A); the release rate of Cur from CN@C emulsion in an environment simulating gastrointestinal digestion in vitro(B)

Cur absorption is completed by passive transport in the small intestine, and a rapid first-pass effect occurs in the small intestine and liver (Yuan et al., 2024). Therefore, if the bioavailability of Cur is to be improved, the adverse effects of gastroal digestion on it must be overcome. We simulated in vitro digestion to evaluate the release of Cur from G1C2@C and CN@C (**Fig. 8B**). As shown in **Fig. 8B**, the release rate of Cur from CN@C emulsion in SCF was less than 15.8%, 84.22% of Cur in CN@C was released into SIF (pH = 6.8) after 3 h of incubation, and 47.80% of Cur entered SGF which was 31% more than that of G1C2@C within 3 h. This was mainly due to the charge interaction and hydrogen bond breakage in the casein molecules, which caused the interface of the CN@C emulsion to be destroyed and Cur to be released into the digestive fluid.

At the same time, the distribution state of the droplets and droplet size of G1C2@C in different digestive fluids (**Fig.8A**). The particle size of GC2@C emulsion changes in a weakly acidic to alkaline environment, which has the potential to release Cur. Interestingly, we found that the release of Cur from GC2@C emulsion in SCF was 80.40% at most, and the droplet size of the GC2@C in SIF and SGF increased from 657.20 nm to 891.44 nm. The structural changes of GPs were completely dependent on the indirect mechanism (microbiota), the β-configuration of the C-2 anomer of the fructose monomer helped GPs resist hydrolysis by human digestive enzymes in the upper gastrointestinal tract (Qiu et al., 2021). These results suggested that the G1C2@C emulsion has potentially pH-responsive and colon-targeted delivery properties, along with a slow-release effect upon reaching the site of action.

4. Conclusions

In this study, GPs and CN were subjected to the Maillard reaction to produce a series of GPs-CN conjugates, which were utilized to enhance the emulsification properties of casein. With a mass ratio of GPs to CN 1:2, GPs-CN conjugates the disordered structure increased by 3.69%. The GPs-CN conjugates showed changes in the secondary structure, the number of hydroxyl groups, the consumption of tryptophan residues and the changes in crystallization properties, which improved the solubility and emulsification properties of CN. Moreover, the G1C2@Cur emulsion prepared by glycosylation modification (DG of GPs and CN was 30.63 ± 1.22%) was stably delivered curcumin. The emulsifying stability of the casein-based emulsion was effectively improved by the glycosylated part in the emulsion system, the emulsion was made more stable. At the same time, G1C2@Cur emulsion was prepared by us using a stable emulsion to encapsulate curcumin. The encapsulation efficiency of G1C2@Cur emulsion was 98.11 ± 0.74%, and the average particle size was 217.1 ± 0.3 nm. G1C2@Cur emulsion was significantly stable and had a pH response potential.

This emulsion study provides a new and more comprehensive analytical solution for the protein emulsion encapsulation strategy, and preparation of stable delivery

emulsions of glycated proteins. Thereby, obtaining a new food-grade surfactant. Although the G1C2@Cur emulsion exhibits a high colon retention rate and potential for sustained release in in vitro gastrointestinal simulations, there is currently a lack of research on the mechanism of its targeted delivery of hydrophobic bioactive substances or even colon-targeted drugs. The limitations of this study remain significant and warrant further exploration.

Credit authorship contribution statement

Xinyan Bai: Writing-original draft, Conceptualization, Data curation. **Lingyu Li**: Data curation, Formal analysis. **X. G. Qiao**: Methodology. **Yiteng Qiao**: Funding acquisition. **Wenqing Zhu**: Investigation. **Laibing Sun &Yanna Hu:** Software. **Zhenjia Zheng**: Conceptualization. **Marie-Laure Fauconnier**: Formal analysis.

Declaration of Competing Interest

The authors declare that they have no known competing financial interests or personal relationships that could have appeared to influence the work reported in this paper.

Acknowledgments

This work was supported by the National Natural Science Foundation of China [No.32202008].

References

Aronson, M. P., & Princen, H. M. (1980). Contact angles associated with thin liquid films in emulsions. *Nature*, *286*(5771), 370-372. https://doi.org/10.1038/286370a0

Ajandouz, E. H., Tchiakpe, L. S., Ore, F. D., Benajiba, A., & Puigserver, A. (2001). Effects of pH on caramelization and Maillard reaction kinetics in fructose-lysine model systems. *Journal of food science*, *66*(7), 926-931. https://doi.org/10.1111/j.1365-2621.2001.tb08213.x

Bai, X., Qiu, Z., Zheng, Z., Song, S., Zhao, R., Lu, X., & Qiao, X. (2022). Preparation and characterization of garlic polysaccharide-Zn (II) complexes and their bioactivities as a zinc supplement in Zn-deficient mice. *Food Chemistry: X*, *15*, 100361. https://doi.org/10.1016/j.fochx.2022.100361

Bo, R., Ji, X., Yang, H., Liu, M., & Li, J. (2021). The characterization of optimal selenized garlic polysaccharides and its immune and antioxidant activity in chickens. *International Journal of Biological Macromolecules*, *182*, 136-143.

Cai, Z., Wei, Y., Shi, A., Zhong, J., Rao, P., Wang, Q., & Zhang, H. (2023). Correlation between interfacial layer properties and physical stability of food emulsions: Current trends, challenges, strategies, and further perspectives. *Advances in Colloid and Interface Science*, *313*, 102863. https://doi.org/10.1016/j.cis.2023.102863

Cui, H., Zang, Z., Jiang, Q., Bao, Y., Wu, Y., Li, J., ... & Li, B. (2023). Utilization of ultrasound and glycation to improve functional properties and encapsulated efficiency of proteins in anthocyanins. *Food Chemistry*, *419*, 135899. https://doi.org/10.1016/j.foodchem.2023.135899

Chen, X., Fan, R., Wang, Y., Munir, M., Li, C., Wang, C., ... & He, J. (2024). Bovine milk β-casein: Structure, properties, isolation, and targeted application of isolated products. *Comprehensive Reviews in Food Science and Food Safety*, *23*(2), e13311.

Ding, Y., Chen, L., Shi, Y., Akhtar, M., Chen, J., & Ettelaie, R. (2021). Emulsifying and emulsion stabilizing properties of soy protein hydrolysates, covalently bonded to polysaccharides: The impact of enzyme choice and the degree of hydrolysis. *Food Hydrocolloids*, *113*, 106519. https://doi.org/10.1016/j.foodhyd.2020.106519

Dadwal, V., & Gupta, M. (2023). Recent developments in citrus bioflavonoid encapsulation to reinforce controlled antioxidant delivery and generate therapeutic uses. *Critical Reviews in Food Science and Nutrition*, *63*(9), 1187-1207. https://doi.org/10.1080/10408398.2021.1961676

Etale, A., Onyianta, A. J., Turner, S. R., & Eichhorn, S. J. (2023). Cellulose: a review of water interactions, applications in composites, and water treatment. *Chemical reviews*, *123*(5), 2016-2048. https://dx.doi.org/10.2139/ssrn.4671395

Fauziee, N. A. M., Chang, L. S., Mustapha, W. A. W., Nor, A. R. M., & Lim, S. J. (2021). Functional polysaccharides of fucoidan, laminaran and alginate from Malaysian brown seaweeds (*Sargassum polycystum*, *Turbinaria ornata* and *Padina boryana*). *International journal of biological macromolecules*, 167, 1135-1145. https://doi.org/10.1016/j.ijbiomac.2020.11.067

Fan, H., Zhu, P., Hui, G., Shen, Y., Yong, Z., Xie, Q., & Wang, M. (2023). Mechanism of synergistic stabilization of emulsions by amorphous taro starch and protein and emulsion stability. *Food Chemistry*, *424*, 136342. https://doi.org/10.1016/j.foodchem.2023.136342

Gowthami, D., & Sharma, R. K. (2023). Influence of hydrophilic and hydrophobic modification of the porous matrix on the thermal performance of form stable phase change materials: a review. *Renewable and Sustainable Energy Reviews*, *185*, 113642. https://doi.org/10.1016/j.rser.2023.113642

Hohmann, Thomas, Suvrat Chowdhary, Kenichi Ataka, Jasmin Er, Gesa Heather Dreyhsig, Joachim Heberle, and Beate Koksch. "Introducing Aliphatic Fluoropeptides: Perspectives on Folding Properties, Membrane Partition and

Proteolytic Stability". *Chemistry–A European Journal* 29, no. 23 (2023): e202203860. https://doi.org/10.1002/chem.202203860

Hussain, Y., Islam, L., Khan, H., Filosa, R., Aschner, M., & Javed, S. (2021). Curcumin–cisplatin chemotherapy: A novel strategy in promoting chemotherapy efficacy and reducing side effects. *Phytotherapy Research*, *35*(12), 6514-6529.

Jiang, Z., Huangfu, Y., Jiang, L., Wang, T., Bao, Y., & Ma, W. (2023). Structure and functional properties of whey protein conjugated with carboxymethyl cellulose through maillard reaction. *LWT*, *174*, 114406. https://doi.org/10.1016/j.lwt.2022.114406

Kara, H. H., Araiza-Calahorra, A., Rigby, N. M., & Sarkar, A. (2024). Flaxseed oleosomes: Responsiveness to physicochemical stresses, tribological shear and storage. *Food Chemistry*, *431*, 137160. https://doi.org/https://doi.org/10.1016/j.foodchem.2023.137160

Karbasi, M., & Askari, G. (2021). Modification of whey protein microgel particles with mono-oligo-and polysaccharides through the Maillard reaction: Effects on structural and techno-functional properties. *Food Structure*, 28, 100184. https://doi.org/10.1021/jf60217a041

Kim, W., Wang, Y., & Selomulya, C. (2020). Dairy and plant proteins as natural food emulsifiers. *Trends in Food Science & Technology*, 105, 261-272. https://doi.org/10.1016/j.tifs.2020.09.012

Kuang, Y., Zhao, S., Liu, P., Liu, M., Wu, K., Liu, Y., ... & Jiang, F. (2023). Schiff base type casein-konjac glucomannan conjugates with improved stability and emulsifying properties via mild covalent cross-linking. *Food Hydrocolloids*, 141, 108733. https://doi.org/10.1016/j.foodhyd.2023.108733

Kumari, N., Kumar, M., Lorenzo, J. M., Sharma, D., Puri, S., Pundir, A., ... & Kennedy, J. F. (2022). Onion and garlic polysaccharides: A review on extraction, characterization, bioactivity, and modifications. *International Journal of Biological Macromolecules*, *219*, 1047-1061.

Lam, R. S., & Nickerson, M. T. (2013). Food proteins: A review on their emulsifying properties using a structure-function approach. *Food Chemistry*, 141(2), 975-984.

Lei, H., Lin, J., Chen, Z., Shi, Z., Niu, D., Zeng, X., ... & Han, Z. (2023). The behavior of whey protein isolate-curcumin complex at the oil-water interface. *Food Hydrocolloids*, *145*, 109046. https://doi.org/10.1016/j.foodhyd.2023.109046

Lin, J., Tang, Z. S., Brennan, C. S., Chandrapala, J., Gao, W., Han, Z., & Zeng, X. A. (2023). Valorizing protein-polysaccharide conjugates from sugar beet pulp as an emulsifier. *International Journal of Biological Macromolecules*, *226*, 679-689. https://doi.org/10.1016/j.ijbiomac.2022.11.217

Lima, R. R., Stephani, R., Perrone, Í. T., & de Carvalho, A. F. (2023). Plant-based proteins: a review of factors modifying the protein structure and affecting emulsifying properties. *Food Chemistry Advances*, 100397. https://doi.org/10.1016/j.focha.2023.100397

Li, C., Peng, H., Cai, J., Li, L., Zhang, J., & Mai, Y. (2021). Emulsion-Guided Controllable Construction of Anisotropic Particles: Droplet Size Determines Particle Structure. *Advanced Materials*, *33*(31), 2102930. https://doi.org/10.1002/adma.202102930

Li, H., Song, J., Liu, C., Wang, X., Liu, Y., Han, M., ... & Gao, Z. (2024). Corn starch/β-Cyclodextrin composite nanoparticles for encapsulation of tea polyphenol and development of oral targeted delivery systems with pH-responsive properties. *Food Hydrocolloids*, *151*, 109823. https://doi.org/10.1016/j.foodhyd.2024.109823

Li, J., Yang, J., Li, J., Gantumur, M. A., Wei, X., Oh, K. C., & Jiang, Z. (2023). Structure and rheological properties of extruded whey protein isolate: Impact of inulin. *International Journal of Biological Macromolecules*, 226, 1570-1578. https://doi.org/10.1016/j.ijbiomac.2022.11.268

Li, M., Wen, X., Wang, K., Liu, Z., & Ni, Y. (2022). Maillard induced glycation of β-casein for enhanced stability of the self-assembly micelles against acidic and

calcium environment. *Food Chemistry*, *387*, 132914. https://doi.org/10.1016/j.foodchem.2022.132914

Li, M., Yu, H., Gantumur, M. A., Guo, L., Lian, L., Wang, B., ... & Jiang, Z. (2024). Insight into oil-water interfacial adsorption of protein particles towards regulating Pickering emulsions: A review. *International Journal of Biological Macromolecules*, 132937. https://doi.org/10.1016/j.ijbiomac.2024.132937

Lima, R. R., Stephani, R., Perrone, Í. T., & de Carvalho, A. F. (2023). Plant-based proteins: a review of factors modifying the protein structure and affecting emulsifying properties. *Food Chemistry Advances*, 100397. https://doi.org/10.1016/j.focha.2023.100397

Li, R., Cui, Q., Wang, G., Liu, J., Chen, S., Wang, X. & Jiang, L. (2019). Relationship between surface functional properties and flexibility of soy protein isolate-glucose conjugates. *Food Hydrocolloids*, 95, 349-357. https://doi.org/10.1016/j.foodhyd.2019.04.030

Liu, K., Zhang, X., Liu, R., Su, W., Song, Y., & Tan, M. (2024). Preparation of Lutein Nanoparticles by Glycosylation of Saccharides and Casein for Protecting Retinal Pigment Epithelial Cells. *Journal of Agricultural and Food Chemistry*, *72*(12), 6347-6359. https://doi.org/10.1021/acs.jafc.3c09054

Liu, Y., Guo, X., Liu, T., Fan, X., Yu, X., & Zhang, J. (2024). Study on the structural characteristics and emulsifying properties of chickpea protein isolate-citrus pectin conjugates prepared by Maillard reaction. *International Journal of Biological Macromolecules*, *264*, 130606. https://doi.org/10.1016/j.ijbiomac.2024.130606

Lu, F., Chi, Y., & Chi, Y. (2024). High-temperature glycosylation of saccharides to modify molecular conformation of egg white protein and its effect on the stability of high internal phase emulsions. *Food Research International*, *176*, 113825. https://doi.org/10.1016/j.foodres.2023.113825

Ma, X., & Chatterton, D. E. (2021). Strategies to improve the physical stability of sodium caseinate stabilized emulsions: A literature review. *Food Hydrocolloids*, *119*, 106853.

Mahdavi, S. A., Jafari, S. M., Assadpoor, E., & Dehnad, D. (2016). Microencapsulation optimization of natural anthocyanins with maltodextrin, gum Arabic and gelatin. *International journal of biological macromolecules*, 85, 379-385. https://doi.org/10.1016/j.ijbiomac.2016.01.011

Meng, Y., & Nicolai, T. (2023). The effect of the contact angle on particle stabilization and bridging in water-in-water emulsions. *Journal of Colloid and Interface Science*, *638*, 506-512. https://doi.org/10.1016/j.jcis.2023.02.006

Nooshkam, M., & Varidi, M. (2020). Whey protein isolate-low acyl gellan gum Maillard-based conjugates with tailored technological functionality and antioxidant activity. *International Dairy Journal*, *109*, 104783. https://doi.org/10.1016/j.idairyj.2020.104783

Nishat, Z. S., Hossain, T., Islam, M. N., Phan, H. P., Wahab, M. A., Moni, M. A., et al. (2022). Hydrogel nanoarchitectonics: an evolving paradigm for ultrasensitive biosensing. *Small*, 18(26), 2107571. https://doi.org/10.1002/smll.202107571

Qiu, Z., Qiao, Y., Zhang, B., Sun-Waterhouse, D., & Zheng, Z. (2022). Bioactive polysaccharides and oligosaccharides from garlic (Allium sativum L.): Production, physicochemical and biological properties, and structure–function relationships. *Comprehensive Reviews in Food Science and Food Safety*, 21(4), 3033-3095. https://doi.org/10.1111/1541-4337.12972.

Qiu, Z., Li, L., Zhu, W., Qiao, X., Zheng, Z., & Sun-Waterhouse, D. (2024). Pectins rich in RG-I and galactose extracted from garlic pomace: Physicochemical, structural, emulsifying and antioxidant properties. *Food Hydrocolloids*, *149*, 109559. https://doi.org/10.1016/j.foodhyd.2023.109559

Qu, D., Wang, S., Zhao, H., Liu, H., Zhu, D., & Jiang, L. (2021). Structure and interfacial adsorption behavior of soy hull polysaccharide at the oil/water interface

as influenced by pH. *Food Hydrocolloids*, 116, 106638. https://doi.org/10.1016/j.foodhyd.2021.106638

Rezvani, H., Binks, B. P., & Nguyen, D. (2024). Surfactant-Nanoparticle Formulations for Enhanced Oil Recovery in Calcite-Rich Rocks. *Langmuir*. https://doi.org/10.1021/acs.langmuir.4c03100

Ribeiro, M. C. (2012). High viscosity of imidazolium ionic liquids with the hydrogen sulfate anion: a Raman spectroscopy study. *The Journal of Physical Chemistry B*, *116*(24), 7281-7290. https://doi.org/10.1021/jp302091d

Saw, R. K., Rane, P. M., Joshi, D., Prakash, S., Jangid, L., & Mandal, A. (2023). Enhanced oil recovery using a novel non-ionic surfactant synthesized from olive oil: Performance and synergistic effects. *Journal of Molecular Liquids*, *392*, 123452. https://doi.org/10.1016/j.molliq.2023.123452

Shang, J., Zhong, F., Zhu, S., Wang, J., Huang, D., & Li, Y. (2020). Structure and physiochemical characteristics of whey protein isolate conjugated with xylose through Maillard reaction at different degrees. *Arabian Journal of Chemistry*, *13*(11), 8051-8059. https://doi.org/10.1016/j.arabjc.2020.09.034

Shao, X., Sun, C., Tang, X., Zhang, X., Han, D., Liang, S., ... & Chen, C. (2020). Anti-inflammatory and intestinal microbiota modulation properties of Jinxiang garlic (Allium sativum L.) polysaccharides toward dextran sodium sulfate-induced colitis. *Journal of Agricultural and Food Chemistry*, *68*(44), 12295-12309.

Spotti, M. J., Loyeau, P. A., Marangon, A., Noir, H., Rubiolo, A. C., & Carrara, C. R. (2019). Influence of Maillard reaction extent on acid induced gels of whey proteins and dextrans. *Food Hydrocolloids*, *91*, 224-231 https://doi.org/10.1016/j.foodhyd.2019.01.020

Sriprablom, J., Luangpituksa, P., Wongkongkatep, J., Pongtharangkul, T., & Suphantharika, M. (2019). Influence of pH and ionic strength on the physical and rheological properties and stability of whey protein stabilized o/w emulsions

containing xanthan gum. *Journal of Food Engineering*, *242*, 141-152. https://doi.org/10.1016/j.jfoodeng.2018.08.031

Sun, Y., Wang, Y., **e, Y., Li, T., Wang, Y., Zhang, X., ... & Dong, W. (2024). Ultra-stable Pickering emulsion stabilized by anisotropic pea protein isolate-fucoidan conjugate particles through Maillard reaction. *International Journal of Biological Macromolecules*, *264*, 130589. https://doi.org/10.1016/j.ijbiomac.2024.130589

Tian, X., Wang, D., Li, Y., Xu, Z., Ren, X., & Kong, Q. (2023). Preparation and characterization of emulsions of soy protein isolate-chitosan quaternary ammonium salt complexes and peppermint essential oil with extended release effect. *Food Hydrocolloids*, *142*, 108779. https://doi.org/10.1016/j.foodhyd.2023.108779

Verma, R., Pyreddy, S., Redmond, C. E., Qazi, F., Khalid, A., O'Brien-Simpson, N. M., & Tomljenovic-Hanic, S. (2023). Detection and identification of amino acids and proteins using their intrinsic fluorescence in the visible light spectrum. *Analytica Chimica Acta*, 1282, 341925. https://doi.org/10.1016/j.aca.2023.341925

Wu, J., Yu, G., Zhang, X., Staiger, M. P., Gupta, T. B., Yao, H., & Wu, X. (2024). A fructan-type garlic polysaccharide upregulates immune responses in macrophage cells and in immunosuppressive mice. *Carbohydrate Polymers*, *344*, 122530.

Wang, S., Zhao, H., Qu, D., Yang, L., Zhu, L., Song, H., & Liu, H. (2022). Destruction of hydrogen bonding and electrostatic interaction in soy hull polysaccharide: Effect on emulsion stability. *Food Hydrocolloids*, *124*, 107304. https://doi.org/10.1016/j.foodhyd.2021.107304

Wang, Y., Li, M., Wen, X., Tao, H., Wang, K., Fu, R., ... & Ni, Y. (2023). Conformational changes and the formation of new bonds achieving robust nanoemulsions by electrostatic interactions between whey protein isolate and chondroitin sulfate. *Food Hydrocolloids*, 136, 108263. https://doi.org/10.1016/j.foodhyd.2022.108263

Wijaya, W., Patel, A. R., Setiowati, A. D., & Van der Meeren, P. (2017). Functional colloids from proteins and polysaccharides for food applications. *Trends in Food Science & Technology*, 68, 56-69. https://doi.org/10.1016/j.tifs.2017.08.003

Wu, J., Xu, F., Wu, Y., Xiong, W., Pan, M., Zhang, N., ... & Wang, L. (2020). Characterization and analysis of an oil-in-water emulsion stabilized by rapeseed protein isolate under pH and ionic stress. *Journal of the Science of Food and Agriculture*, *100*(13), 4734-4744. https://doi.org/10.1002/jsfa.10532

Xu, G., Wang, C., & Yao, P. (2017). Stable emulsion produced from casein and soy polysaccharide compacted complex for protection and oral delivery of curcumin. *Food Hydrocolloids*, 71, 108-117. https://doi.org/10.1016/j.foodhyd.2017.05.010

Yan, Y., Hang, F., Wei, T., **e, C., & Niu, D. (2022). Modification of ovalbumin by Maillard reaction: effect of heating temperature and different monosaccharides. *Frontiers in Nutrition*, *9*, 914416. https://doi.org/10.3389/fnut.2022.914416

Yang, H., Su, Z., Meng, X., Zhang, X., Kennedy, J. F., & Liu, B. (2020). Fabrication and characterization of Pickering emulsion stabilized by soy protein isolate-chitosan nanoparticles. *Carbohydrate polymers*, 247, 116712. https://doi.org/10.1016/j.carbpol.2020.116712

Yang, F., Yang, J., Qiu, S., Xu, W., & Wang, Y. (2021). Tannic acid enhanced the physical and oxidative stability of chitin particles stabilized oil in water emulsion. *Food Chemistry*, *346*, 128762. https://doi.org/10.1016/j.foodchem.2020.128762

Yang, Y., Gupta, V. K., Du, Y., Aghbashlo, M., Show, P. L., Pan, J., ... & Rajaei, A. (2023). Potential application of polysaccharide mucilages as a substitute for emulsifiers: A review. *International journal of biological macromolecules*, 124800. https://doi.org/10.1016/j.ijbiomac.2023.124800

Yao, Z. F., Wang, J. Y., & Pei, J. (2023). Controlling morphology and microstructure of conjugated polymers via solution-state aggregation. *Progress in Polymer Science, 136*, 101626. https://doi.org/10.1016/j.progpolymsci.2022.101626

Zhao, J., Chang, B., Hu, Y., Wang, X., Cao, Z., Zhang, Y., ... & Sui, X. (2024). Adsorption mechanism of soy protein amyloid fibrils with different morphological structures at the interface of oil-in-water emulsion. *Food Hydrocolloids*, 110899. https://doi.org/10.1016/j.foodhyd.2024.110899

Zhao, W., Chi, Y., & Chi, Y. (2023). Saccharides alleviate the thermal instability behavior of liquid egg yolk: Influence on rheology property, emulsifying property and protein conformation. *Food Hydrocolloids*, *143*, 108853. https://doi.org/10.1016/j.foodhyd.2023.108853

Zhang, Y., Zhang, Y., Chen, N., Xin, N., Li, Q., Ye, H., ... & Zhang, T. (2022). Glycated modification of the protein from Rana chensinensis eggs by Millard reaction and its stability analysis in curcumin encapsulated emulsion system. *Food Chemistry, 382*, 132299. https://doi.org/10.1016/j.foodchem.2022.132299

Zhang, Z., Wang, B., & Adhikari, B. (2022). Maillard reaction between pea protein isolate and maltodextrin via wet-heating route for emulsion stabilisation. *Future Foods, 6*, 100193. https://doi.org/10.1016/j.fufo.2022.100193

Zhang, M., Wang, L., Liu, Y., & Li, J. (2022). Effects of antioxidants, proteins, and their combination on emulsion oxidation. *Critical Reviews in Food Science and Nutrition, 62*(29), 8137-8160. https://doi.org/10.1080/10408398.2021.1925869

Zheng, L., Cao, C., Li, R., Cao, L., Zhou, Z., Li, M., et al. (2018). Preparation and characterization of water-in-oil emulsions of isoprothiolane. *Colloids and Surfaces A:Physicochemical and Engineering Aspects,* 537, 399–410. https://doi.org/10.1016/j.colsurfa.2017.10.031

Figure captions

Fig. 1 ESI and EAI of the GPs∶CN ratios ranged at pH 7(A, B), pH 4.6(D, E) at 70 °C; FT-IR(C), Fluorescence(F) of the GPs∶CN = 6:1, 4:1, 2:1, 1:1, 1:2, 1:4, 1:6

Fig. 2 XRD of the GPs∶CN ratios ranged from different samples

Fig. 3 Contact angle the CN(A) and at the GPs∶CN ratios of 6∶1(B), 4:1(C), 2:1(D), 1:1(E), 1:2(F), 1:4(G), 1:6(H) at pH 7

Fig. 4. TEM image of CN emulsion(A), G6C1 emulsion(B), G4C1 emulsion(C), G2C1 emulsion(D), G1C1 emulsion(E), G1C2 emulsion(F), G1C4 emulsion(G) and G1C6 emulsion(H)

Fig. 5 (A) Changes in the storage modulus during heating from 25°C–90 °C; (B) The Compound viscosity in different temperatures; (C) LF-NMR for emulsions; (D) The energy Loss modulus during heating from 25°C–90°C; (E) Apparent viscosity and stress as a function of shear rate for emulsions; (F) Details in LF-NMR for emulsions

Fig.6 Average particle size and PDI (A), and zeta potential (B) of CN and GPs-CN conjugates; Drug LC (C) and LE (D) at Different addition amounts of curcumin emulsion**;** Particle size potential and zeta potential of CN@Cur emulsion and G1C2@Cur emulsion at different temperatures (E) and pH (F). Different letters mean values showed significant differences ($p < 0.05$).

Fig. 7 Viscosity of CN@Cur emulsion and G1C2@Cur at different temperatures (A) and different pH (B); appearance photograph of the emulsions stabilized by CN@Cur (C(a)) and G1C2@Cur (C(b)) with different pH; TSI, T and BS spectra of CN@Cur (D(a)) and G1C2@Cur(D(b)) emulsions for 24 h. Insert photographs of emulsions after 15 h.

Fig. 8 The distribution state of the droplets and droplet size of G1C2@C in different digestive fluids(A); the release rate of Cur from CN@C emulsion in an environment simulating gastrointestinal digestion *in vitro*(B)

Declaration of interests

☒ The authors declare that they have no known competing financial interests or personal relationships that could have appeared to influence the work reported in this paper.

☐ The authors declare the following financial interests/personal relationships which may be considered as potential competing interests:

Highlights

- Garlic polysaccharide-casein (GPs-CN) conjugates have emulsifying potential
- G1C2 emulsion has high stability, especially thermal stability
- G1C2 emulsion can be made into an oil-in-water emulsion for encapsulation
- G1C2@C emulsions showed great pH response and targeted delivery potential

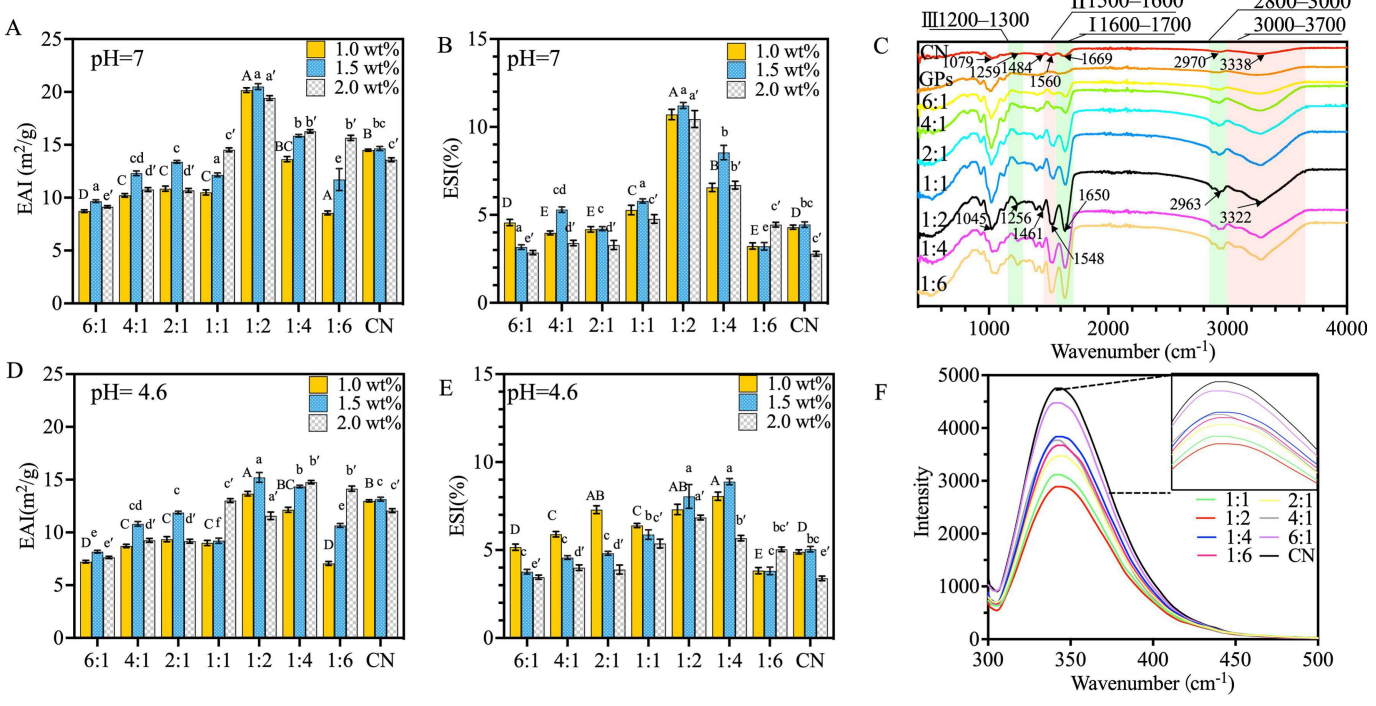
A
pH=7
1.0 wt%
1.5 wt%
2.0 wt%
EAI (m²/g)
6:1 4:1 2:1 1:1 1:2 1:4 1:6 CN
B
pH=7
ESI(%)
C
Ⅲ1200–1300
Ⅱ1500–1600
Ⅰ1600–1700
2800–3000
3000–3700
CN
GPs
6:1
4:1
2:1
1:1
1:2
1:4
1:6
1079
1259
1484
1560
1669
2970
3338
1650
2963
3322
1045
1256
1461
1548
Wavenumber (cm⁻¹)
D
pH= 4.6
EAI(m²/g)
E
pH=4.6
ESI(%)
F
Intensity
1:1
1:2
1:4
1:6
2:1
4:1
6:1
CN
Wavenumber (cm⁻¹)

Figure 1

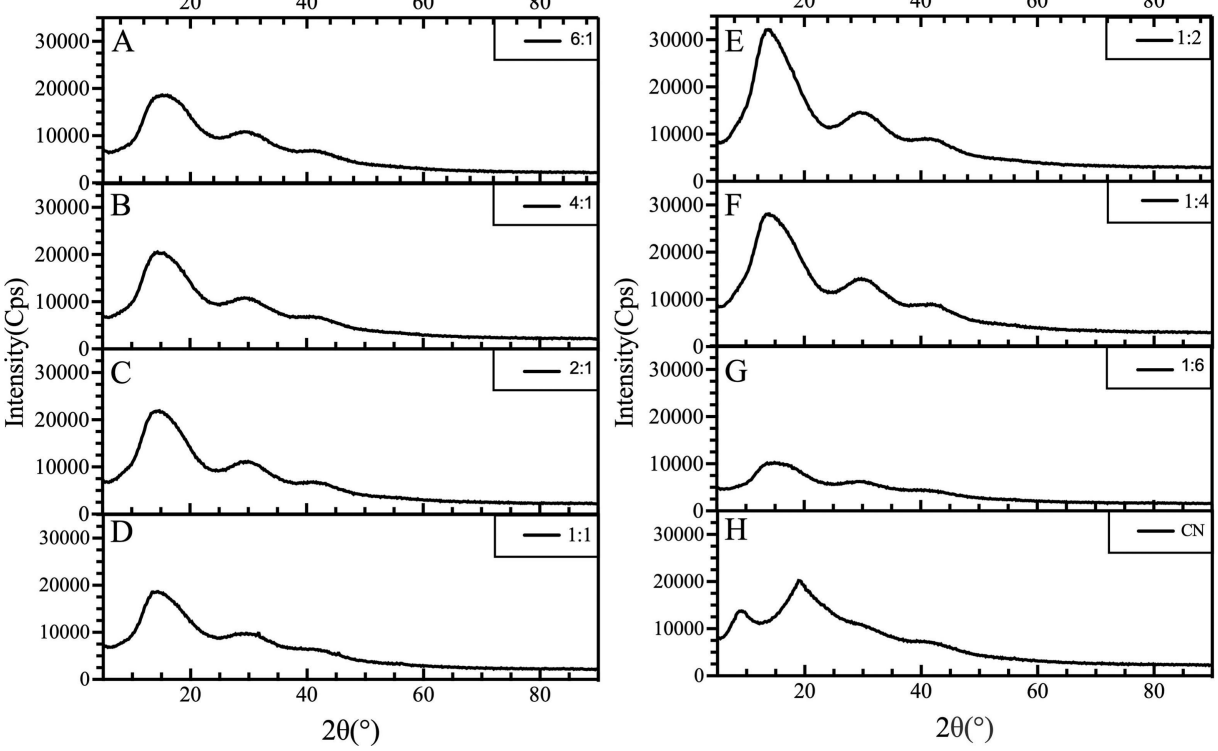
A
6:1
B
4:1
C
2:1
D
1:1
E
1:2
F
1:4
G
1:6
H
CN
Intensity(Cps)
2θ(°)
0
10000
20000
30000
20
40
60
80

Figure 2

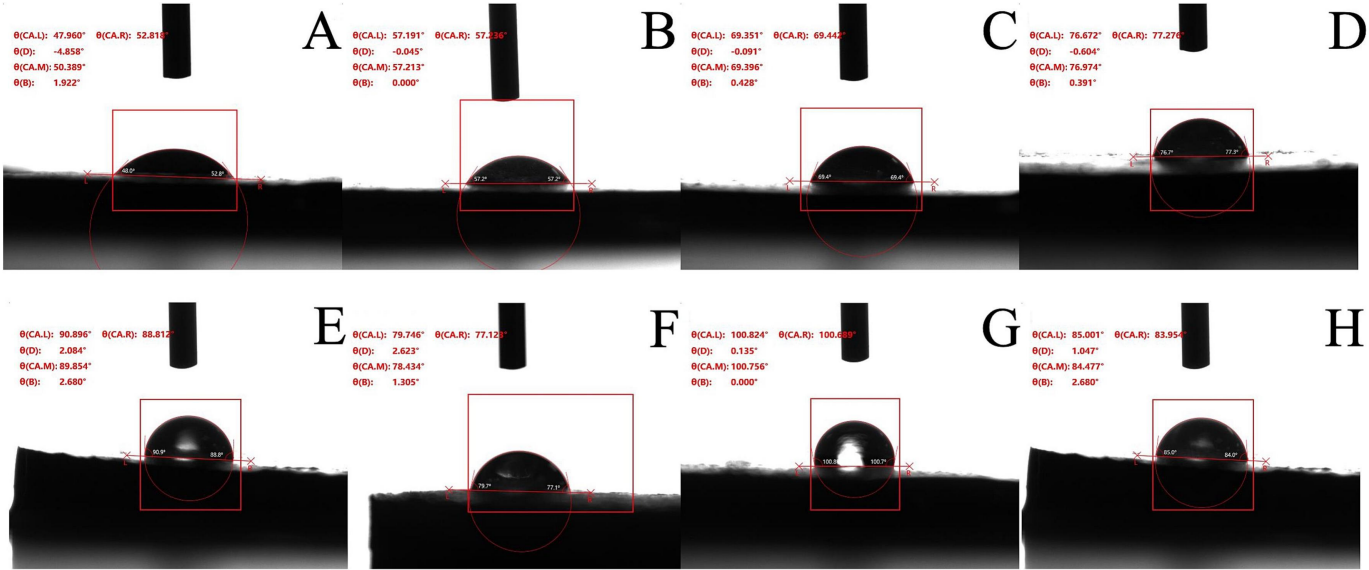
θ(CA.L): 47.960° θ(CA.R): 52.814°
θ(D): -4.858°
θ(CA.M): 50.389°
θ(B): 1.922°
A
θ(CA.L): 57.191° θ(CA.R): 57.236°
θ(D): -0.045°
θ(CA.M): 57.213°
θ(B): 0.000°
B
θ(CA.L): 69.351° θ(CA.R): 69.442°
θ(D): -0.091°
θ(CA.M): 69.396°
θ(B): 0.428°
C
θ(CA.L): 76.672° θ(CA.R): 77.276°
θ(D): -0.604°
θ(CA.M): 76.974°
θ(B): 0.391°
D
θ(CA.L): 90.896° θ(CA.R): 88.812°
θ(D): 2.084°
θ(CA.M): 89.854°
θ(B): 2.680°
E
θ(CA.L): 79.746° θ(CA.R): 77.123°
θ(D): 2.623°
θ(CA.M): 78.434°
θ(B): 1.305°
F
θ(CA.L): 100.824° θ(CA.R): 100.689°
θ(D): 0.135°
θ(CA.M): 100.756°
θ(B): 0.000°
G
θ(CA.L): 85.001° θ(CA.R): 83.954°
θ(D): 1.047°
θ(CA.M): 84.477°
θ(B): 2.680°
H

Figure 3

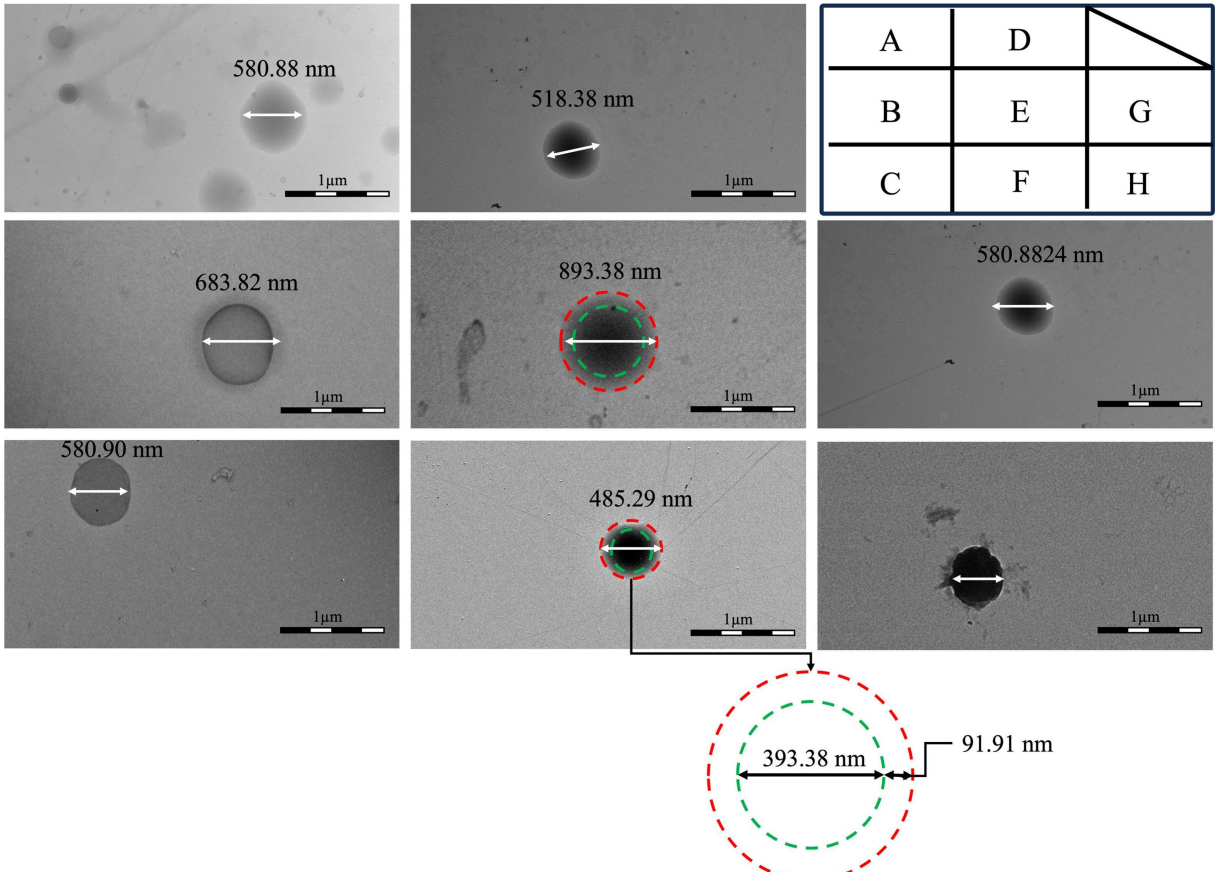
580.88 nm
1μm
518.38 nm
1μm
A
D
B
E
G
C
F
H
683.82 nm
1μm
893.38 nm
1μm
580.8824 nm
1μm
580.90 nm
1μm
485.29 nm
1μm
1μm
393.38 nm
91.91 nm

Figure 4

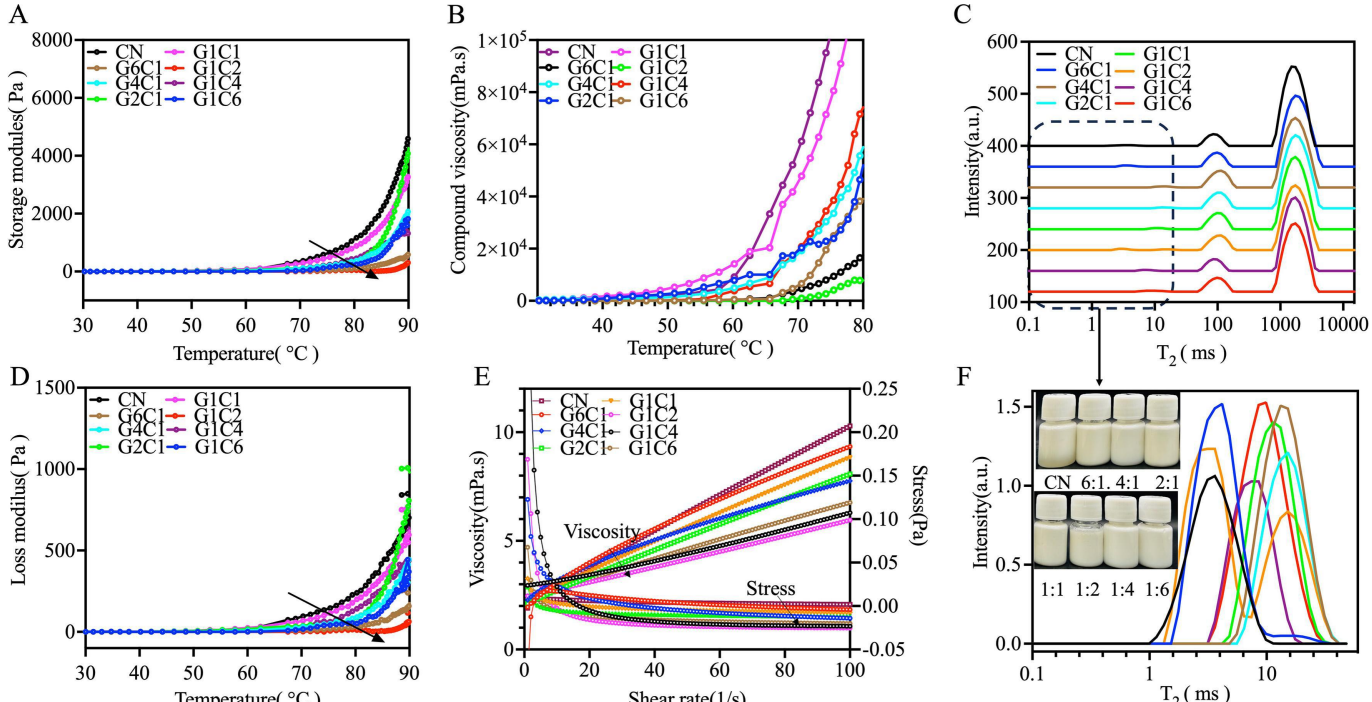
A
Storage modules(Pa)
Temperature(°C)
CN
G6C1
G4C1
G2C1
G1C1
G1C2
G1C4
G1C6
B
Compound viscosity(mPa.s)
Temperature(°C)
C
Intensity(a.u.)
T2 (ms)
D
Loss modulus(Pa)
Temperature(°C)
E
Viscosity(mPa.s)
Stress(Pa)
Viscosity
Stress
Shear rate(1/s)
F
Intensity(a.u.)
T2 (ms)
CN 6:1. 4:1 2:1
1:1 1:2 1:4 1:6

Figure 5

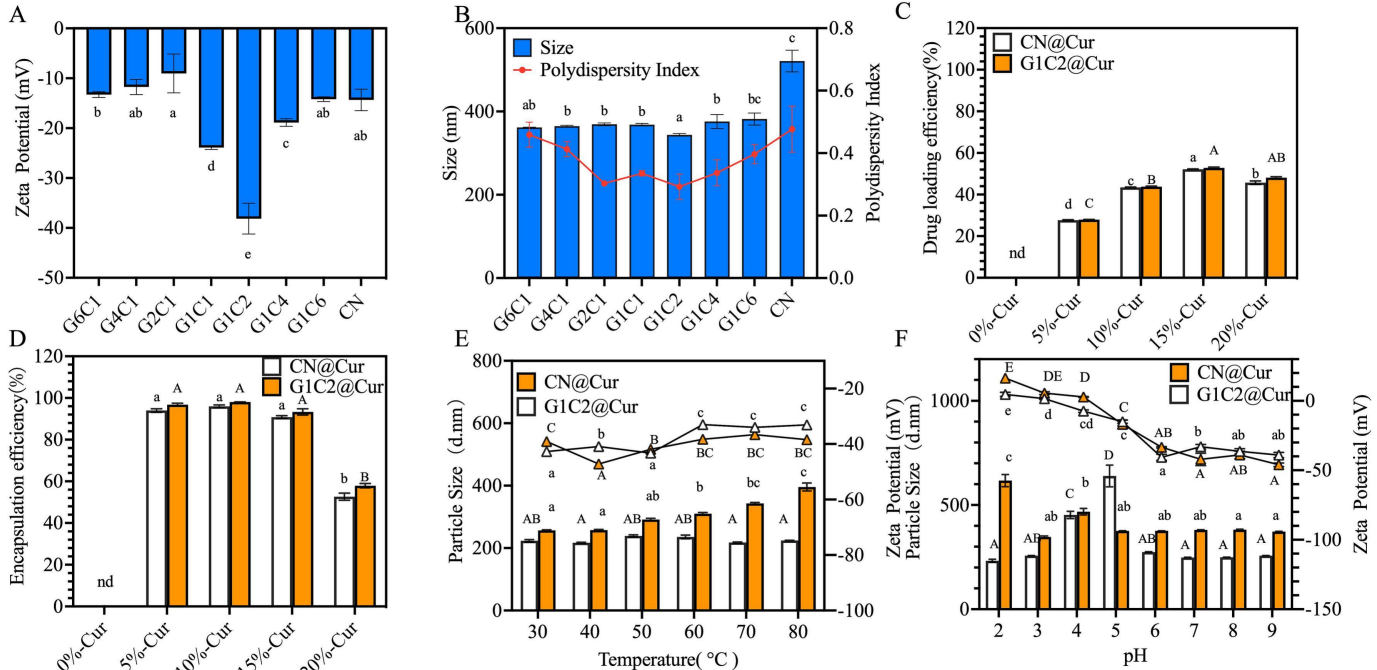
A
Zeta Potential (mV)
G6C1
G4C1
G2C1
G1C1
G1C2
G1C4
G1C6
CN
B
Size
Polydispersity Index
Size (nm)
Polydispersity Index
C
CN@Cur
G1C2@Cur
Drug loading efficiency(%)
nd
0%-Cur
5%-Cur
10%-Cur
15%-Cur
20%-Cur
D
Encapsulation efficiency(%)
E
Particle Size (d.nm)
Temperature(°C)
F
Zeta Potential (mV)
Particle Size (d.nm)
pH

Figure 6

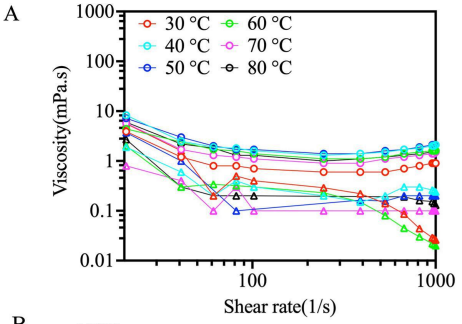

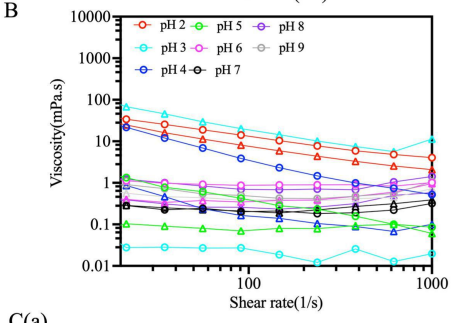

C(a)

C(b)

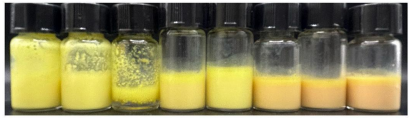

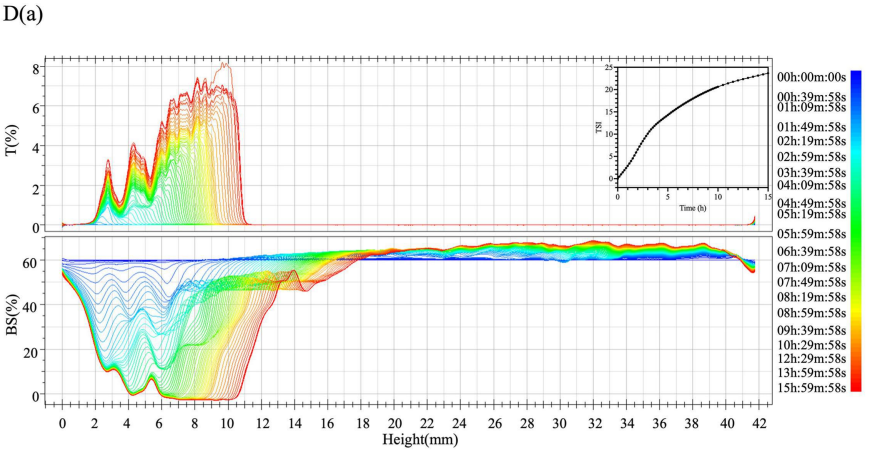

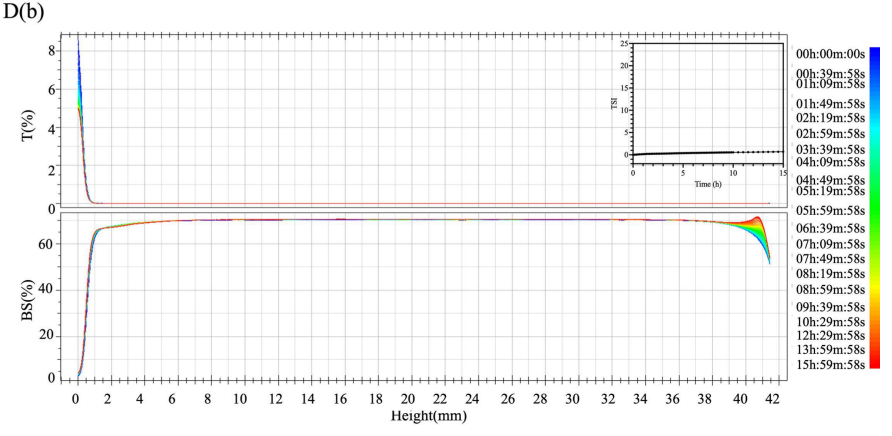

Figure 7

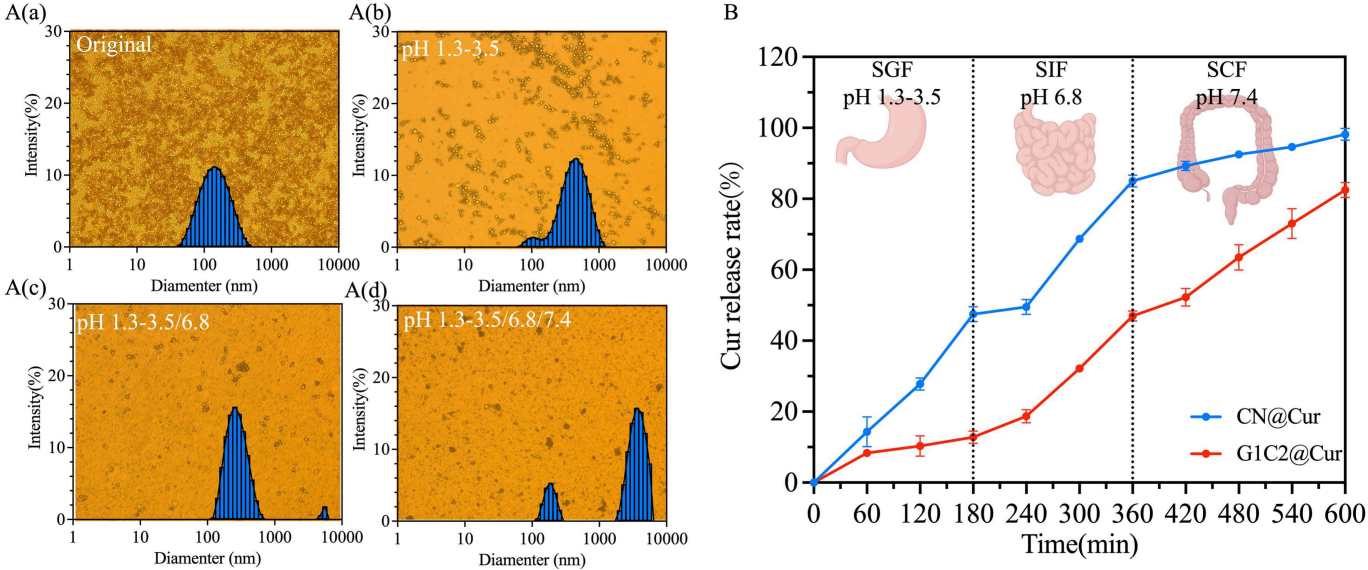
A(a)
Original
A(b)
pH 1.3-3.5
A(c)
pH 1.3-3.5/6.8
A(d)
pH 1.3-3.5/6.8/7.4
Intensity(%)
Diamenter (nm)
B
SGF
pH 1.3-3.5
SIF
pH 6.8
SCF
pH 7.4
Cur release rate(%)
Time(min)
CN@Cur
G1C2@Cur

Figure 8